Fine structure of the Gamow-Teller resonance revealed in the decay of ^{150}Ho 2^- isomer

A. Algora,* B. Rubio, D. Cano-Ott, J. L. Taín, A. Gadea, and J. Agramunt
IFIC, CSIC-Univ. Valencia, Apartado Oficial 22085, 46071 Valencia, Spain

M. Gierlik, M. Karny, Z. Janas, A. Płochocki, K. Rykaczewski, and J. Szerypo
Institute of Experimental Physics, Warsaw University, PL-00-681, Warsaw, Poland

R. Collatz, J. Gerl, M. Górska, H. Grawe, M. Hellström, Z. Hu, R. Kirchner, M. Rejmund, E. Roeckl, M. Shibata, and GSI Euroball Collaboration
Gessellschaft für Schwerionenforschung, D-64220 Darmstadt, Germany

L. Batist
St. Petersburg Nuclear Physics Institute, 188-350 Gatchina, Russia

J. Blomqvist
Royal Institute of Technology, SE-10 691 Stockholm, Sweden

(Received 11 March 2003; revised manuscript received 23 May 2003; published 5 September 2003)

The γ rays following the 72*s* ^{150}Ho 2^- Gamow-Teller β decay have been investigated with the CLUSTER CUBE setup, an array of six EUROBALL CLUSTER Ge detectors in close cubic geometry, providing a γ ray detection sensitivity of 2×10^{-5} per β-parent decay for γ-ray energies up to 5 MeV. The fine structure of the Gamow-Teller resonance at 4.4-MeV excitation in ^{150}Dy has been studied. The resolved levels are compared with Shell Model predictions.

DOI: 10.1103/PhysRevC.68.034301 PACS number(s): 21.10.Pc, 21.60.Cs, 23.20.Lv, 23.40.Hc

I. INTRODUCTION

Studies of β decay provide an important element in our understanding of nuclear structure. The process itself is relatively simple since the $\sigma\tau$ operator, which is responsible for the decay in most of the cases (Gamow-Teller decays), allows both the nuclear spin and isospin to change by only one unit. The same operator governs the closely related, charge-exchange reactions. Here, however, there are serious experimental difficulties, both in terms of the interpretation of the background in the ejectile spectra and the absolute normalization. Such studies have also been limited up to now to reactions with stable beams and stable targets. β-decay studies, on the other hand, are relatively free of background uncertainties. Moreover, in principle, they allow the study of more than 6000 species in the Chart of the Nuclides. At the same time they also have a fundamental, inherent limitation, namely, the limited Q_β window accessible in the decay. This limitation must be kept in mind if we want to compare the experimental β-decay probability with theoretical estimates, since the agreement may be highly sensitive to the accuracy of the calculations inside the energy window. This is a very delicate problem in general.

The present work describes one of the several experiments in which we attempt to understand the Gamow-Teller (GT) β-decays in heavy spherical nuclei. The results presented here concern nuclei in the rare-earth region. They have been reported briefly in conferences [1,2]. Results for nuclei near ^{100}Sn using similar high-sensitivity techniques have also been presented previously [3,4].

It is worth noting here that the experimental determination of the β decay probability is difficult and can only be achieved satisfactorily with the use of a total absorption spectrometer [5]. Measurements of this kind were also part of our experimental program; the results will be presented in a separate paper [6]. The total absorption method cannot, however, provide detailed information about the fine structure of the β intensity distribution as a function of energy. This is partly because of the intrinsically low-energy resolution of the scintillation detector, which is at the core of a total absorption spectrometer, and partly because of the uncertainties in the deconvolution of the spectra.

The alternative is to use a set of high efficiency, composite Ge detectors placed in close geometry around the radioactive source to measure the γ's emitted following the β decay. Measurements of this kind provide the central theme of the present study. They exploit the spectacular improvement in efficiency of composite Ge detectors, which has been achieved in the last decade. This development was motivated originally by in-beam γ-ray studies of fast rotating nuclei, but so far it has seldom been exploited to study β decay. In this method, the β decay feeding (related to the β decay probability) is determined from the balance between the γ's feeding and deexciting the levels in the daugther nucleus. Thus each level is examined individually. In some cases, as happens here, information about the spins and parities of the levels can be extracted. The fraction of the β feeding remaining unobserved in this kind of experiment is an important piece of information, which can be obtained rarely. In this particular case it is possible because we can

*On leave from the Institute of Nuclear Research, Debrecen, Hungary.

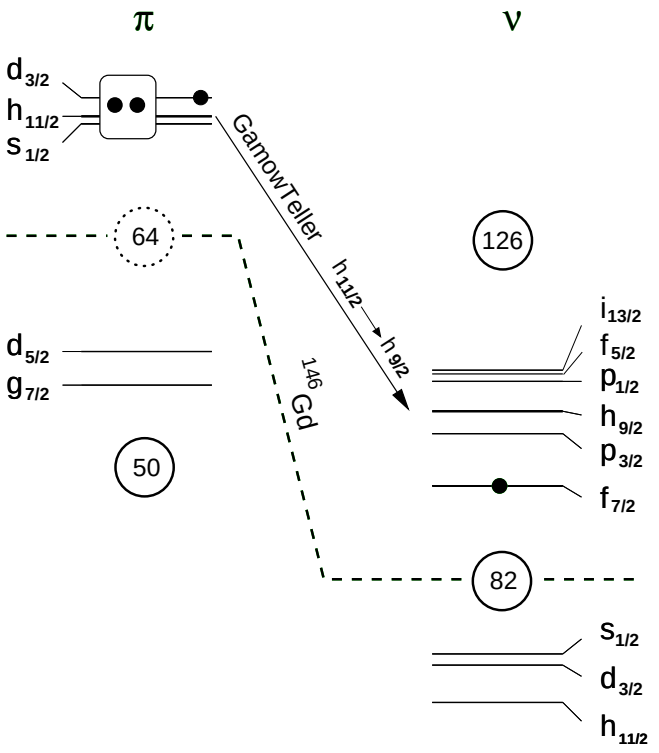

FIG. 1. Schematic view of the single-particle orbitals available in the Gd region. The proposed configuration of the ^{150}Ho 2^- isomer is shown with dots indicating the relevant orbitals. The rounded box is intended to remind the reader that the pair of protons coupled to 0^+ can scatter between the orbitals $s_{1/2}$, $h_{11/2}$, and $d_{3/2}$ due to pairing.

compare the present results with the total absorption data. This comparison is presented in the discussion below. These two experimental approaches to determining the β-strength distribution should ideally converge to the same solution. The comparison made here of the state of the art for the two methods should tell us how well we have succeeded so far.

II. THE ^{150}Ho 2^- CASE

It is of particular interest to study β decays where the GT strength is expected to lie within the Q_β window. In heavy nuclei, this does not happen very often. Above the particle stable $N\sim Z$ nuclei these cases are essentially limited to the nuclei where the GT decay involving the $\pi h_{11/2}\rightarrow\nu h_{9/2}$ or the $\pi g_{9/2}\rightarrow\nu h_{7/2}$ transitions can occur inside the window. In both cases the spin-orbit splitting and the Coulomb repulsion shift the single-particle energy of the two orbitals in such a way that there are cases where the proton high j orbit is being filled while the neutron low j orbital is empty and not far away from the Fermi surface.

Amongst these cases the decay of the ^{150}Ho 2^- isomer is an ideal candidate for the study of the GT resonance and its fine structure because the strength is expected to lie at high excitation energy but still inside the Q_β window. The parent ^{150}Ho is a nucleus with four particles above the ^{146}Gd core and has an isomeric state with $I^\pi=2^-$ (it is not clear whether it is an isomer or the ground state, but this is experimentally not clarified and irrelevant to the present discussion). Considering the single-particle proton orbitals between $Z=64$ and 82 (Fig. 1), and the fact that the $\nu f_{7/2}$ orbit is considerably lower in energy than the other single-particle neutron orbitals in the 82–126 shell, the most probable configuration for the 2^- state is $(\pi d_{3/2}\nu f_{7/2})_{2^-}(\pi^2)_{0^+}$. Consequently this will be considered as the main 2^- parent state configuration. The β decay of the unpaired proton is forbidden, consequently the decay will proceed through the breakup of the 0^+ pair. However, this disintegration will only occur when the two protons are in the $\pi\ h_{11/2}$ orbital and the decay will populate states of four-particle character of the configuration $[(\pi d_{3/2}\nu f_{7/2})_{2^-}(\pi h_{11/2}\nu h_{9/2})_{1^+}]1^-,2^-,3^-$. In this case the first part of the wave function remains unaltered with respect to the parent state and the 0^+ proton pair changes. A crude approximation to the excitation energy of these states is twice the pairing gap for protons plus twice the pairing gap for neutrons in the even-even daughter nucleus ^{150}Dy plus the neutron $h_{9/2}$ single-particle energy, i.e., at $\approx$5 MeV excitation energy. This decay is very similar to the decay of ^{148}Dy, which is simpler because ^{148}Dy has the 0^+ proton pair above the ^{146}Gd core. The present case should be much the same and should have a comparable $\log_{10} ft$ [i.e., 3.95(3) [7]], except for the blocking effect caused by the presence of the $\pi\ d_{3/2}$ particle in the parent state, which should modify the probability of the $\pi\ h_{11/2}$ pair in ^{150}Ho with respect to the ^{148}Dy case. Summarizing, in the β decay of the ^{150}Ho 2^- state we expect to populate levels at $\approx$5 MeV in ^{150}Dy with a total $\log_{10} ft$ value near 3.9.

III. EXPERIMENTS

From the point of view of the experiment, $^{150}\mathrm{Ho}_{83}$ 2^- is a favorable case. On one hand, it is an odd-odd nucleus and consequently has a Q_β value ($\sim$7 MeV) higher than $^{150}\mathrm{Er}_{82}$ ($\sim$5 MeV) or $^{150}\mathrm{Dy}_{84}$ ($\sim$3 MeV), the two main isobaric contaminants. The other possible nucleus produced, $^{150}\mathrm{Tm}_{81}$, was observed with only 0.3% intensity of the total ^{150}Ho 2^- production. On the other hand, the ^{150}Ho 2^- parent can be produced in a very clean way using the $0^+(\mathrm{GT})\rightarrow 1^+(E1)\rightarrow 2^-$ decay sequence (see Fig. 2). In other words, our aim is to produce ^{150}Er directly by a ^{96}Ru(^{58}Ni,4p) reaction, and the ^{150}Ho 2^- isomer, the object of our study, only as a β-decay product. This method avoids the complications associated with the direct production of ^{150}Ho in the nuclear reaction which will inevitably produce the 9^+ β isomer in the same nucleus as well. The direct population of the 9^+ isomer was not completely avoided in our experiment because of other Ru isotopes present in the 96.52% enriched ^{96}Ru target. As a result, the corresponding decay lines were clearly visible in the spectra and were taken into account in the analysis.

The ^{150}Er activity was produced in the 4p exit channel of the fusion-evaporation reaction induced by a ^{58}Ni beam, accelerated in the GSI-Unilac up to 5.3 MeV/u, impinging on a 2-mg cm^{-2} ^{96}Ru target. Typical beam intensities were of the order of 30 p-nA. The recoiling nuclei were stopped and ionized in a thermal ion source, extracted as singly charged ions by 55 kV voltage, and separated in the GSI on-line mass

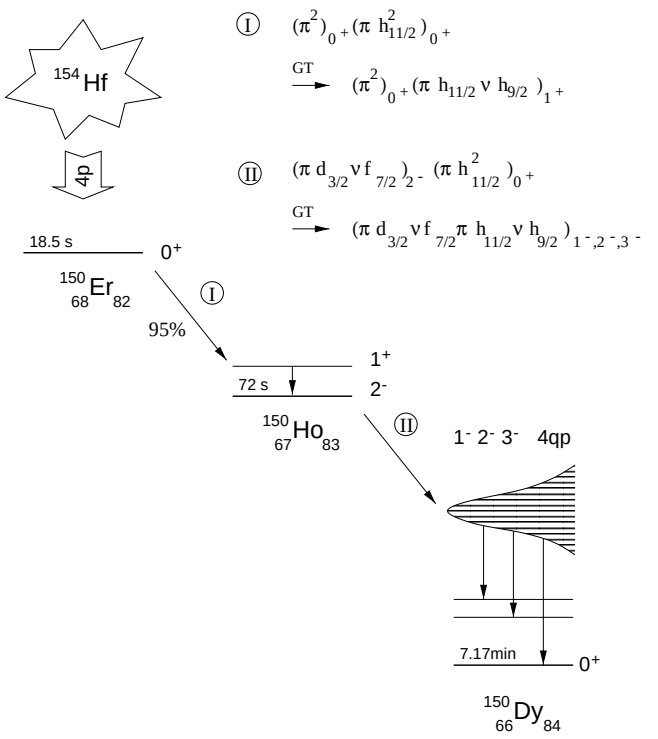

FIG. 2. Production mechanism for the ^{150}Ho 2^- isomer.

separator. The mass-separated activity was deposited on a tape transport system with a differential pumping system which allowed it to pass from the mass-separator vacuum to atmospheric pressure. The samples were collected for 120 s and transported to the measuring site, about 2 m away, where they remained for 120 s while the next sample was collected. The cycle was optimized to measure the ^{150}Ho 2^- decay with its 72-s half-life. The intensity of the ^{150}Er beam was of the order of 2000 atoms/s with a fresh thermal ion source, which typically decreased to half the intensity after 4 h of ^{58}Ni irradiation, and was therefore changed every 12 h.

The mass-150 samples were placed in the middle of the ''CLUSTER CUBE'' detector setup consisting of six EUROBALL CLUSTER detectors [8] in compact geometry (Fig. 3). The distance from the sample position to the central crystal of the CLUSTER detectors was 10.2 cm for four CLUSTER detectors in a symmetric ring and 11.3 cm for the other two. The different distances were caused by geometrical constraints on the setup.

A particular problem in this kind of experiment, in contrast with typical in-beam experiments with heavy ions and Ge arrays, is the expected low multiplicity of the γ cascades in β decay, which prevents triggering with high fold events. Moreover, we were specifically interested in measuring singles, which for the 42 detectors was only possible in list mode. Consequently the rate of events to be written on tape was in some cases too high and the acquisition dead time significant.

In order to overcome this difficulty we used a trigger where the rate of single-hit events could be reduced by a given factor, if necessary. In the present experiment, however, this possibility was not used. In other words all kinds of

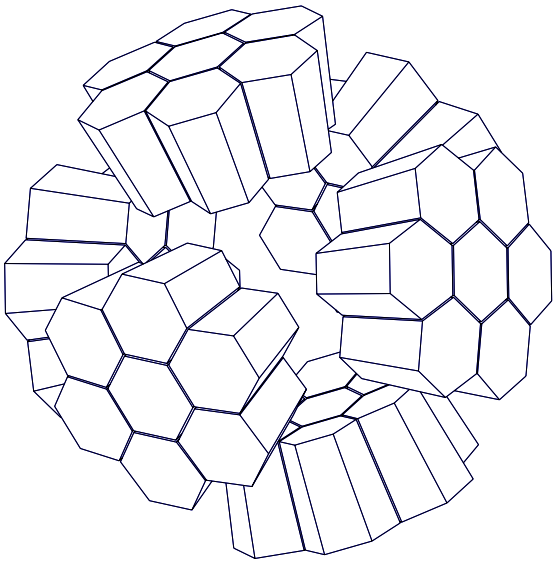

FIG. 3. The CLUSTER CUBE setup used in the experiment.

events, including single hits, were written on tape without any reduction. The ^{150}Ho 2^- decay trigger rate was typically 8 kHz and the acquisition system had a dead time of $\sim$70 μs. We recorded 6.5×10^8 events in total and 4.0×10^8 γ-γ coincidences within a measuring time of 31 h.

In parallel with the complex coincidence and total-singles electronics, we took direct spectra for two central and two peripheral capsules of the CLUSTER detectors. This allowed us to control the status of the ion source and to determine absolute efficiencies without dead-time ambiguities.

Efficiencies and energies were calibrated carefully. For efficiency determination, sources of ^{152}Eu, ^{133}Ba, ^{56}Co, and an absolutely calibrated mixed source (AMERSHAM E0898) were used. The lines from the sources cover γ-ray energies from 53 keV to 3.451 MeV. The estimated uncertainty of the photopeak efficiency within this interval was 5%. In order to estimate the efficiency above this energy, we have performed Monte Carlo simulations using GEANT 3. Further details of the efficiency calibration can be found in Ref. [4].

For energy calibration we have measured the mass-150 activity together with ^{56}Co and ^{16}O sources. Special attention was devoted to obtaining an energy calibration valid over a wide range of energy. For the high-energy part of the spectra the transitions of ^{56}Co and the full-energy, single-escape, and double-escape peaks of the 6.128-MeV $E3$ transition in ^{16}O were used. To obtain the energies of transitions corresponding to the mass-150 activity we used the direct histograms measured with Silena H7421 analog-to-digital converters (ADCs) because they were more linear than those used in the list-mode data acquisition system. The calibration provided accurate energies from 475 to 6128 keV with less than 0.25-keV deviation.

The energies obtained in this way were used to calibrate internally the full statistics singles spectrum. The latter was created by adding the spectra from all 42 capsules and all of the runs. To do this without losing resolution and maintaining an accurate energy calibration over the full-energy range

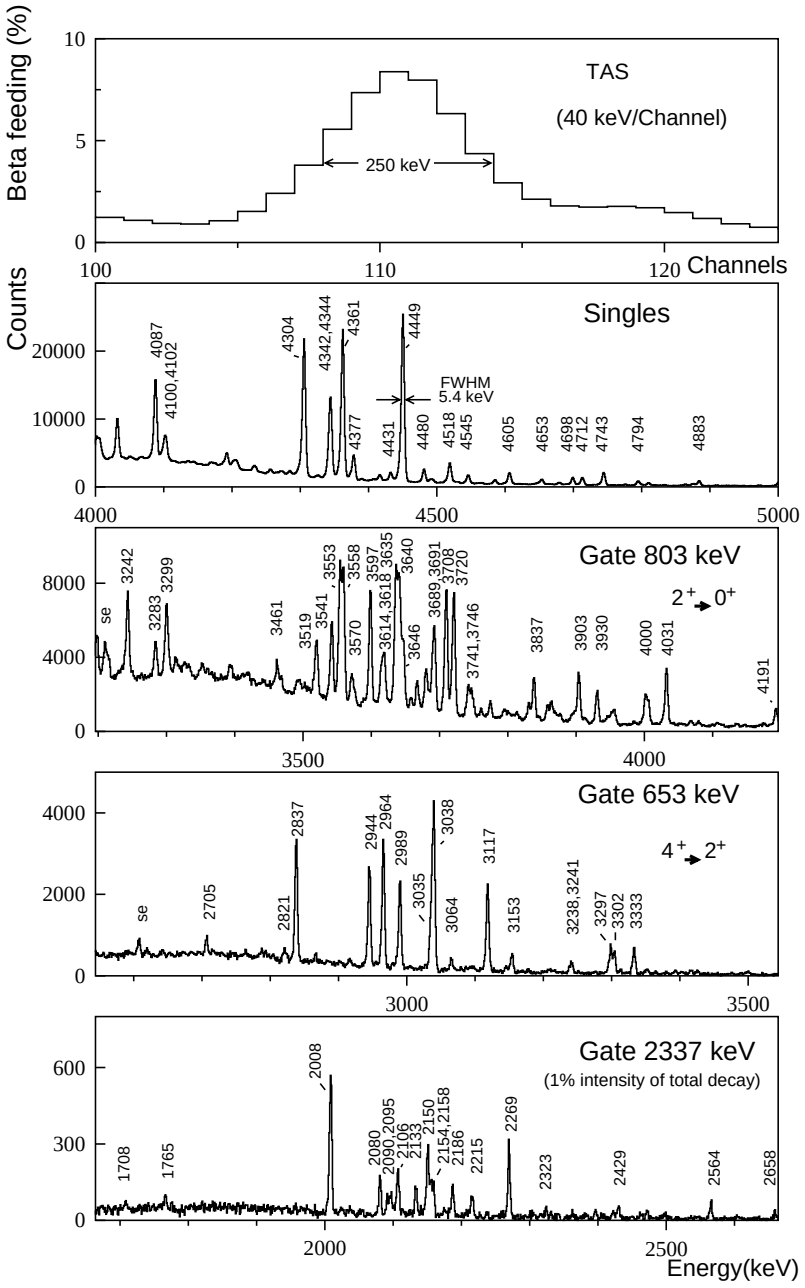

FIG. 4. Comparison of different spectra, obtained in the analysis of the decay of the ^{150}Ho 2^- isomer, in the region of the resonance. In the topmost panel the β feeding obtained with the total absorption spectrometer (TAS) [2,6] is presented for comparison. The other panels show CLUSTER CUBE data. In the second panel, the singles spectrum is presented. The position of the resonance is clearly seen in the gated spectra (see 803-, 653-, 2337-keV gates). It is even seen in the weaker 2337-keV gate which represents 1% of the intensity of the total decay (note that the region shown in the spectra are shifted accordingly to the energy of the gate).

was difficult because of the strong nonlinearities of the ADCs and the small shifts in gain occurring during a measurement time of several days. To tackle this problem we first corrected the nonlinearities for each detector using several calibration sources and three energy ranges for each detector and then used several internal calibration lines to match the 42 detectors and correct for small shifts during the experiment. The energy resolution obtained in this way was 3.2 keV at 1.332 MeV, 5.4 keV at the resonance energy (4.4 MeV) (see Fig. 4), and 6.8 keV at 7.6 MeV (the 7631.7 and 7645.5-keV doublet in ^{57}Fe, a contaminant in our spectra coming from *n* capture, was clearly resolved). The estimated uncertainty in γ-energy determination over the range 0.1–7.65 MeV is below 0.5 keV.

In order to establish the ^{150}Ho 2^- decay scheme we constructed two different matrices. A γ-γ coincidence matrix between the 42 individual Ge capsules and an add-back–add-back matrix where we add the events occurring simultaneously in two or three neighboring crystals of a CLUSTER detector. The add-back factor for γ's of 4 MeV was 1.7 and the background reduction factor at low energies (200 keV) was 3. Both matrices presented advantages and disadvantages. The add-back matrix had better efficiency at high energies and lower background at low energies, but the summing effect was relatively strong due to the large solid angle. It also had slightly worse energy resolution. The single capsule matrix was very sensitive to single-escape and double-escape peaks. Most of these effects could be clearly identified by comparison of the two matrices.

The results are given in the form of a compact table (Table I) where each level and its deexcitation pattern are specified with energies and intensities. The level energies

TABLE I. Levels in ^{150}Dy with their corresponding decay pattern. The first column shows the energy of the levels in keV with their estimated uncertainty (see text). E_γ and I_γ represent the energy (in keV) and intensity of γ transitions deexiting the levels. The intensities are quoted relative to the 803.7-keV transition (equivalent to 12 514 parent decay).

$E_{level}(\Delta E)$	$E_\gamma(I_\gamma)$
803.6(0.2)	803.7(10000)
1395.0(0.2)	591.6(2546)
1456.9(0.2)	653.5(1805)
1786.3(0.2)	1786.2(309), 983.1(541)
1893.0(0.3)	1089.4(132)
1983.1(0.2)	1983.2(211), 1180.1(402)
2051.2(0.3)	656.8(357)
2186.8(0.4)	792.2(37.0), 730.4(26.7)
2226.0(0.2)	1422.3(109), 831.5(161), 243.5(7.1)
2253.7(0.4)	1449.9(40.4)
2317.6(0.3)	1514.2(99.2), 425.3(1.9)
2321.6(0.2)	927.0(286), 535.7(18.1), 427.9(0.5), 338.6(8.5)
2330.8(0.3)	1527.1(48.4), 874.2(163)
2337.0(0.3)	2337.2(167), 1533.2(25.0), 942.5(4.3)
2346.6(0.3)	2346.6(171), 1542.8(26.6), 560.9(19.0), 453.9(1.2), 363.8(6.2)
2411.9(0.3)	1608.9(149), 1017.2(7.8), 955.5(59.0), 625.4(3.0)
2419.0(0.4)	1023.7(4.8), 962.2(34.0), 232.2(0.6)
2434.8(0.4)	1631.2(47.2), 1040.4(3.0)
2460.9(0.3)	2460.9(43.2), 1657.0(110), 1066.2(30.0)
2509.7(1.0)	1706.0(4.0)
2521.0(0.3)	1717.4(61.0), 1126.6(26.5), 1064.5(79.5), 734.0(35.8), 538.1(7.9), 470.1(7.0)
2529.1(0.3)	2529.2(115), 1725.4(25.7), 1134.5(38.2), 1072.1(5.0)
2618.4(0.4)	1814.8(59.9), 1161.8(17.5)
2635.3(1.0)	1240.3(5.9)
2671.6(0.4)	1868.0(58.2), 885.6(1.2)
2697.0(0.3)	1302.4(7.6), 1240.4(52.1), 366.5(10.8)
2713.6(0.3)	2713.3(102), 1910.2(14.0), 1319.0(39.2), 927.4(5.5)
2740.8(0.3)	1937.6(16.2), 1345.8(2.9), 1284.3(40.7), 954.6(6.5), 757.9(5.5)
2800.6(0.3)	2800.2(60.0), 1997.4(16.9), 1014.4(11.8), 818.0(1.3)
2836.5(0.7)	2033.4(34.7), 1049.6(1.4)
2844.9(0.3)	2041.3(109), 1449.6(62.7), 1058.4(3.7), 862.0(8.1)
2855.8(0.4)	2051.7(15.8), 1399.2(33.8), 1069.0(8.0), 872.8(4.1)
2910.9(1.1)	724.1(1.4)
2928.2(1.0)	1141.8(5.6)
2930.3(0.3)	879.1(41.9), 744.0(0.9), 704.1(6.8)
2943.9(0.4)	1548.9(61.1), 1486.8(10.6), 525.2(5.5)
2946.8(1.0)	1489.8(4.2)
2955.6(0.3)	2152.1(67.8), 1560.9(10.4), 1499.0(14.8), 972.6(2.6), 904.3(4.0), 769.1(3.0), 730.2(5.9), 634.0(1.8), 625.0(2.7)
2972.0(0.3)	2972.0(21.0), 2168.5(40.2), 1185.9(5.7)
2979.8(0.3)	2175.9(70.1), 996.7(3.5)
3005.9(0.3)	1610.7(55.3), 1220.0(22.0), 1022.8(1.6), 818.7(1.0), 780.0(6.0), 684.0(8.8)
3010.4(0.5)	2206.8(17.2), 673.3(2.1)
3038.6(0.3)	3039.0(27.7), 2234.7(21.1), 1643.7(32.9)
3067.9(0.7)	737.1(4.2)
3069.2(0.3)	3069.4(32.5)
3082.8(1.0)	1031.5(2.6)
3101.8(0.3)	2298.2(37.2), 1315.3(2.5)
3107.9(1.0)	1651.0(2.1)
3112.5(0.4)	2308.7(11.0), 1655.6(17.3), 1326.6(9.8), 1129.1(4.9), 859.3(4.2), 781.2(1.9)
3131.4(0.4)	2327.9(16.5), 1345.4(8.8), 785.0(1.6), 610.7(7.6)
3133.8(1.0)	1676.9(3.0)

TABLE I. (*Continued*).

$E_{level}(\Delta E)$	$E_\gamma(I_\gamma)$
3141.0(1.0)	2337.4(4.0)
3150.4(0.4)	1755.2(11.2), 1099.4(2.9), 963.7(16.0), 731.0(3.0)
3151.9(0.6)	1695.0(2.6), 925.6(11.8), 830.6(2.4)
3156.4(0.4)	1761.5(20.3), 1699.2(5.9), 1105.6(12.6), 835.1(3.8)
3172.7(0.5)	2368.9(31.5), 1777.5(8.7), 946.8(10.3), 835.9(1.8)
3177.2(0.4)	1781.8(17.5), 1126.4(9.6), 990.8(1.7), 951.3(13.7), 855.6(1.9)
3183.3(0.4)	2379.3(37.0), 1132.1(4.0)
3194.3(0.8)	2391.0(7.0)
3197.6(0.7)	2393.5(3.4)
3199.0(0.4)	1742.4(10.6), 787.4(8.2)
3257.9(1.0)	1862.9(17.0)
3279.2(0.5)	3279.6(18.8)
3292.3(0.4)	2488.6(25.9), 1897.4(8.0), 1240.8(6.5), 1066.7(2.5), 955.4(1.1)
3294.2(0.6)	1107.1(1.2), 1068.5(8.9), 875.1(1.4)
3304.8(0.5)	1909.6(31.1), 1253.8(5.8), 1078.8(10.1), 967.7(2.2)
3326.4(1.0)	1540.1(1.6)
3335.4(0.5)	3335.0(3.0), 1548.7(2.8), 1442.4(2.0), 1005.4(1.6)
3339.5(0.3)	3339.6(28.0), 2535.6(8.5), 1446.8(10.9), 904.5(1.3)
3348.8(1.0)	1891.9(11.4)
3356.3(0.5)	1961.8(12.3), 1305.6(3.4), 1129.9(3.6), 1018.8(2.7)
3366.2(1.0)	845.2(4.7)
3378.8(0.4)	2574.6(3.1), 1983.3(7.2), 1921.9(27.2)
3383.1(0.5)	2579.5(6.0), 1988.0(4.0), 1926.6(8.4), 1399.8(1.7)
3394.9(1.0)	1938.0(5.8)
3405.1(0.6)	2009.7(2.2), 1948.3(4.1), 1354.1(3.4)
3412.9(1.0)	1956.0(2.9)
3414.3(0.7)	2019.3(1.4), 1363.1(3.5)
3422.6(1.0)	2619.0(7.3)
3440.6(0.7)	2637.1(6.1), 1109.7(2.1)
3441.0(1.0)	1389.8(6.2)
3458.7(0.4)	2655.8(17.5), 2064.0(3.0), 2001.3(2.4), 1271.4(1.0), 1127.3(1.1)
3464.5(1.0)	1133.7(2.6)
3465.2(1.0)	2070.3(5.0)
3466.9(1.0)	2010.0(2.8)
3473.7(1.0)	2078.8(3.3)
3480.5(0.6)	2677.0(11.2)
3496.1(1.0)	2692.4(7.8)
3497.0(0.7)	1270.7(3.9), 1166.3(2.3)
3500.6(0.4)	2105.2(12.8), 1714.4(9.2), 1517.3(3.3), 1274.4(4.3), 1163.7(3.5)
3528.6(0.6)	2134.2(2.5), 2070.9(19.0)
3529.4(0.7)	2725.6(14.5), 1303.4(4.2)
3530.3(0.7)	1744.2(2.3), 1199.3(2.0)
3535.7(0.4)	2731.8(47.1), 1749.5(4.7), 1214.1(2.8), 1198.9(1.9)
3542.2(1.0)	1755.9(1.2)
3550.2(1.0)	2155.2(9.9)
3565.0(1.0)	2170.0(5.0)
3567.5(0.4)	2172.6(13.0), 2110.6(14.4), 1583.7(1.8), 1516.0(9.3), 1342.0(5.6), 722.7(2.8), 637.2(1.1)
3577.7(1.0)	2774.1(9.5)
3586.1(1.0)	1534.8(4.1)
3588.9(0.6)	3589.1(12.7), 2194.0(28.5), 1537.3(5.7)
3600.6(0.6)	1549.1(9.4), 1374.8(2.9)
3613.1(1.0)	1561.8(2.7)
3638.6(0.7)	2243.6(3.5), 1587.4(1.1)

TABLE I. (*Continued*).

$E_{level}(\Delta E)$	$E_\gamma(I_\gamma)$
3654.6(0.7)	2851.0(68.7), 1428.6(4.2)
3660.3(0.7)	2265.8(15.1), 1608.4(7.2)
3690.5(0.5)	2886.8(55.1), 2295.6(10.0), 2233.4(4.5), 1639.5(3.5), 1271.4(1.2), 760.5(5.6)
3693.4(1.1)	848.6(2.2)
3704.2(0.4)	2900.4(33.4), 2309.2(84.8), 2247.2(8.1), 1720.9(13.8), 1652.6(3.9), 1382.7(6.1), 859.6(6.3), 848.7(0.5), 760.6(15.7), 724.4(2.4)
3724.0(1.0)	2329.1(5.9)
3733.1(0.4)	2929.1(19.6), 2338.4(9.7), 2276.3(11.4), 1750.2(12.6), 1507.1(4.0), 1402.2(13.2)
3743.5(1.0)	2286.6(3.4)
3749.7(0.6)	1766.4(12.6), 1402.9(1.6), 1009.2(2.5)
3766.6(0.6)	2371.1(6.6), 1540.8(2.2), 1354.8(4.4)
3782.8(1.0)	2387.8(4.0)
3789.1(0.7)	1562.8(5.4), 1452.1(3.3)
3792.6(0.5)	2397.2(17.0), 2006.3(13.8), 1899.6(18.6), 1121.3(2.6)
3804.1(0.6)	3803.9(21.3), 2409.3(6.1), 2347.2(7.1)
3812.8(0.7)	3009.5(3.3), 2355.4(4.2)
3834.2(0.8)	3834.2(10.0), 1940.8(0.8), 1373.8(2.6)
3857.8(0.3)	3857.8(23.4), 3054.5(11.7), 2462.8(111), 2400.9(40.4), 2071.4(10.6), 1965.0(7.8), 1874.6(11.7), 1807.4(1.3), 1631.4(4.1), 1535.9(8.0), 1526.5(2.6), 1520.8(2.1), 1328.8(2.8), 1161.2(2.8), 1117.3(2.5), 927.0(2.9), 913.6(2.6)
3870.0(0.5)	2474.8(4.3), 2412.7(7.1), 1644.1(4.6), 926.4(8.6)
3873.5(0.4)	3069.8(17.0), 2478.9(8.9), 2087.7(4.9), 1551.5(5.3), 1132.8(1.4), 1028.4(2.4)
3892.2(1.0)	2497.2(3.6)
3895.6(0.6)	3895.5(25.5), 3092.0(15.3), 1558.7(1.9)
3900.8(0.7)	2506.0(2.0), 2443.6(3.5)
3903.7(1.0)	2508.7(5.2)
3916.0(0.4)	3112.6(16.8), 2520.8(15.5), 2459.2(16.9), 2129.7(14.6), 1932.8(4.5), 1864.7(3.2), 1689.9(2.9), 985.8(2.9), 935.8(0.9)
3924.2(0.4)	2529.0(24.4), 2467.0(6.9), 2138.3(10.5), 1872.7(7.4), 1697.8(14.6), 1602.4(15.9), 1577.3(1.9), 1079.6(3.6), 980.1(11.4), 945.0(2.8)
3926.9(1.0)	3123.3(16.7)
3929.8(1.0)	2143.4(5.0)
3968.4(0.6)	2573.6(14.9), 2511.4(4.4), 1742.2(6.9)
3980.9(0.7)	2524.2(2.0), 1997.5(0.6)
4000.3(0.6)	2605.4(7.4), 2214.3(7.3), 1653.3(1.9)
4009.3(1.0)	2116.4(1.3)
4045.8(0.4)	3242.1(43.6), 2650.7(11.3), 1707.8(1.2), 1584.6(3.1), 1246.0(0.3), 863.2(0.8)
4052.6(1.0)	1706.0(1.4)
4086.8(0.5)	4087.1(91.2), 3282.9(31.1), 2193.9(1.4), 2103.5(1.8), 1373.6(1.7)
4099.9(0.4)	4100.3(22.3), 2206.3(1.9), 2117.0(2.0), 1846.0(6.2), 1753.8(3.9), 1638.9(4.0)
4102.3(0.4)	4102.2(38.2), 3298.7(37.0), 2707.0(6.6), 2209.3(11.1), 1848.7(2.8), 1785.0(4.7), 1765.2(1.5), 1573.0(7.1), 1130.8(1.3), 918.5(1.3)
4116.6(1.0)	3313.0(14.0)
4118.8(0.7)	2723.7(5.5), 1772.4(2.8)
4129.1(0.7)	3325.4(14.3), 1798.4(2.3)
4151.5(1.0)	2756.6(4.6)
4154.0(0.6)	2171.1(8.5), 1413.3(3.1), 1115.1(2.2)
4162.7(0.6)	2767.9(5.1), 2705.5(7.6), 1841.2(1.7)
4170.6(0.5)	2713.0(2.0), 2384.1(4.6), 2278.2(1.9), 1916.7(4.7), 1101.8(2.0)
4196.6(1.0)	3392.9(10.1)
4199.0(1.0)	4199.0(4.7)
4208.4(1.0)	1877.6(2.0)
4216.3(1.0)	2821.4(2.0)
4220.6(0.4)	2763.4(2.2), 1899.0(5.2), 1890.0(3.5), 1874.5(2.7), 1808.4(5.1), 1523.9(4.3), 1479.9(3.8), 927.6(0.9)

TABLE I. (*Continued*).

$E_{level}(\Delta E)$	$E_\gamma(I_\gamma)$
4224.3(0.7)	2829.1(4.7), 1907.0(1.7)
4233.8(1.0)	4233.8(4.0)
4253.5(0.7)	2858.5(4.2), 2270.3(2.1)
4255.4(1.0)	4255.4(5.2)
4264.5(1.0)	3460.9(12.6)
4270.3(1.0)	3466.7(6.1)
4278.4(1.0)	2821.4(2.2)
4293.7(0.5)	3490.3(10.0), 2898.6(5.0), 2837.0(50.5), 2507.2(11.1), 1972.0(2.1)
4304.9(0.4)	4304.6(163), 2518.3(10.1), 1983.6(2.8), 1870.3(1.2), 1844.1(4.4), 1591.4(2.5), 965.4(0.4)
4311.4(1.0)	1964.8(1.3)
4322.0(0.7)	3518.7(29.3), 2926.7(3.9)
4340.2(0.7)	2018.0(0.2), 2003.7(1.0)
4342.3(1.0)	4342.3(32.0)
4344.6(0.5)	4344.0(73.0), 3540.8(39.4), 2451.9(35.1), 2361.4(70.2), 2090.0(6.1), 2026.5(1.7), 2022.7(11.3), 2007.6(17.6), 1998.0(7.7), 1909.9(8.4), 1883.4(10.5), 1815.4(15.4), 1673.1(26.5), 1631.1(13.6), 1543.9(1.1), 1373.3(8.0), 1365.5(6.9), 1335.0(15), 1305.8(1.2), 1274.8(2.5), 1242.6(0.3), 1150.1(3.2), 1005.1(1.7), 844.3(5.7), 816.0(3.9)
4355.2(0.7)	4355.0(6.2)
4356.6(0.3)	3552.9(61.6), 2961.4(22.8), 2569.9(28.2), 2305.3(2.0), 2130.4(4.8), 2035.2(4.7), 2010.0(5.9), 1895.8(6.1), 1835.8(3.9), 1827.2(2.1), 1643.2(5.8), 1385.2(3.3), 1318.2(3.1), 1287.5(3.1), 1173.8(1.4)
4361.5(0.4)	4361.3(182), 3557.9(65.5), 2379.1(3.1), 2107.7(3.3), 2015.5(2.3), 1927.0(2.7), 1689.8(3.8), 1351.0(1.2), 1177.4(0.6), 1022.1(0.5), 982.8(1.7)
4373.4(0.6)	3569.8(12.5), 2321.9(8.3), 2051.9(3.5)
4377.4(0.5)	4377.3(24.0), 3573.5(6.1), 1916.5(2.4), 1706.2(1.8), 1275.7(0.3)
4389.6(0.5)	2406.8(5.8), 2071.6(1.9), 1928.4(1.7), 1676.5(2.0)
4401.0(0.3)	3597.4(56.6), 2944.0(44.1), 2614.8(11.4), 2417.8(25.8), 2070.3(19.4), 1989.0(29.3), 1982.1(0.9), 1940.0(5.8), 1880.1(6.1), 1782.5(1.4), 1703.7(4.5), 1600.8(0.8), 1556.2(3.5), 1545.1(0.7), 1470.9(3.5), 1457.0(7.2), 1445.6(1.9), 1421.2(3.7), 1395.8(7.8), 1362.7(3.0), 1270.1(0.9), 1250.3(1.0), 1201.8(1.1), 1108.8(3.4), 1021.6(1.4), 942.0(1.1), 899.9(1.0)
4417.1(0.4)	3613.6(17.5), 2631.2(5.5), 2190.6(4.1), 2099.3(5.8), 2079.9(4.5), 1956.7(0.7), 1887.9(9.8), 1676.6(1.7), 1444.7(1.0), 1378.5(0.7)
4421.6(0.3)	3617.8(25.0), 3026.5(235), 2964.5(53.5), 2438.3(4.2), 2369.8(9.5), 2195.7(12.2), 2099.8(10.3), 2090.6(18.7), 2009.8(6.2), 1961.1(2.0), 1900.4(16.9), 1892.3(16.5), 1803.2(10.9), 1725.0(1.6), 1707.8(14.7), 1681.2(1.5), 1621.4(1.0), 1576.4(8.3), 1491.1(10.4), 1466.1(2.5), 1449.0(0.8), 1415.4(3.2), 1353.8(1.6), 1309.4(3.9), 1290.1(1.7), 1271.2(1.6), 1265.6(2.3), 1244.7(0.5), 1222.6(1.4), 1042.7(6.7), 962.6(2.3), 941.0(1.1), 920.9(1.0), 821.1(8.0)
4427.0(0.3)	3623.2(2.3), 3032.1(37.6), 2443.8(12.7), 2201.0(11.0), 2090.3(2.0), 1966.3(4.7), 1471.4(1.7), 1421.1(4.0), 1358.1(0.9), 1270.5(2.7), 1244.2(1.9), 1087.8(0.4), 1048.3(1.3), 925.8(1.5)
4429.1(1.1)	1449.3(3.2)
4431.6(0.4)	4431.6(11.3), 2538.2(1.1), 2113.8(1.1), 2095.2(2.5), 1902.7(3.6), 1760.0(4.4), 1717.8(2.4), 1393.2(2.0), 1362.6(0.6)
4439.1(0.4)	3634.8(64.5), 3043.6(5.1), 2213.7(7.1), 2117.5(2.5), 2108.4(2.5), 1820.4(1.3), 1742.3(1.0), 1594.2(2.7), 1459.3(2.2), 1240.6(0.6)
4443.1(0.3)	3639.7(62.9), 3048.0(9.7), 2655.8(7.0), 2391.6(3.6), 2121.9(5.3), 2106.1(5.7), 1921.6(2.1), 1487.9(1.0), 1470.6(0.6), 1463.5(3.6), 1404.3(4.0), 1374.0(2.7), 1064.1(4.4), 942.7(2.0), 907.5(1.5)
4444.2(1.0)	4444.2(8.7)
4445.8(0.3)	2988.9(38.0), 2659.7(10.1), 2462.2(5.9), 2394.5(11.9), 2219.7(2.3), 2033.9(24.7), 2027.2(1.1), 1924.6(8.4), 1916.7(4.7), 1827.8(3.8), 1749.1(1.3), 1601.0(8.5), 1589.9(0.2), 1343.9(0.5), 1289.8(1.7), 1167.0(0.2), 1105.9(0.6), 1067.7(1.4)
4449.6(0.4)	4449.4(210), 3645.5(34.5), 2132.0(4.0), 1778.0(1.3), 1380.9(0.9), 1110.1(0.7), 913.7(1.2)
4460.6(0.5)	3656.9(4.2), 2409.3(4.7), 2234.7(4.8), 2139.1(3.9)
4469.6(0.5)	3666.1(12.1), 2152.0(3.3), 2132.6(3.1), 1129.9(0.2)
4480.5(0.5)	4480.3(16.9), 2587.9(2.3), 2045.8(2.5), 1808.7(1.6)
4482.6(0.3)	3678.8(18.7), 3087.9(8.6), 2695.6(20.5), 2499.5(9.1), 2296.6(0.8), 2161.2(5.8), 2152.1(2.8), 2071.4(5.2), 2021.2(2.1), 1768.5(5.2), 1741.6(3.3), 1526.8(1.0), 1502.8(2.0), 1476.6(1.5), 1380.8(1.0), 1298.9(1.8), 1284.6(1.8), 1190.9(0.7)
4486.6(0.3)	3683.0(5.1), 2435.7(3.6), 2261.0(3.1), 2168.5(6.9), 2164.5(2.5), 2149.8(8.7), 2140.0(2.9), 2025.0(2.9), 1965.4(23.5), 1868.2(0.8), 1773.0(7.8), 1506.2(2.4), 1480.6(4.4), 1384.9(1.6), 1374.4(2.4), 1355.7(0.4), 1194.6(0.6)

TABLE I. (*Continued*).

$E_{level}(\Delta E)$	$E_\gamma(I_\gamma)$
4487.8(0.5)	4488.0(3.3), 2504.5(3.3), 1643.00(2.1), 1515.9(0.6)
4491.7(0.3)	3688.7(17.8), 3096.3(23.2), 3034.6(22.8), 2705.4(48.7), 2508.8(23.8), 2440.2(7.0), 2305.5(0.5), 2265.6(7.8), 2170.6(6.6), 2161.0(16.7), 2154.4(3.7), 2079.4(38.8), 2030.6(7.7), 1971.2(9.6), 1962.4(6.7), 1873.4(5.3), 1778.1(6.3), 1561.4(5.5), 1536.0(5.8), 1511.3(2.5), 1485.8(8.1), 1390.3(0.5), 1314.7(1.0), 1199.4(0.7), 1112.5(1.3)
4495.5(0.3)	3691.4(33.0), 3100.4(27.9), 3038.4(68.2), 2512.3(23.4), 2444.3(12.9), 2269.3(27.7), 2164.6(12.3), 2158.5(2.9), 2148.8(11.7), 2083.5(34.6), 2034.7(2.6), 1974.5(22.7), 1877.1(6.4), 1798.4(11.8), 1781.6(15.9), 1754.3(2.5), 1694.5(0.8), 1639.8(1.1), 1565.1(8.0), 1551.4(14.9), 1540.2(3.7), 1394.1(0.6), 1383.4(2.8), 1296.9(0.7), 1216.2(0.5), 1203.2(0.4), 1116.9(1.5)
4511.6(0.3)	4512.5(1.7), 3708.4(63.1), 2725.7(5.6), 2527.8(3.3), 2459.5(3.3), 2285.7(3.8), 2194.3(1.4), 2189.4(3.1), 1983.2(2.6), 1814.3(1.3), 1710.3(0.4), 1473.4(1.0)
4518.4(0.4)	4518.1(25.8), 2625.6(2.6), 2196.4(2.4), 2172.2(1.2), 1846.8(5.1), 1335.5(0.8)
4519.5(0.8)	3124.9(3.2), 1513.2(2.3)
4521.6(0.4)	3064.1(4.4), 2735.3(9.2), 2295.6(7.3), 2190.8(4.0), 2001.0(3.5), 1676.4(3.5), 1550.2(1.0)
4523.5(0.4)	3719.5(62.0), 3128.6(3.3), 2539.8(3.1), 2186.3(3.5), 1810.4(3.8), 1422.0(0.2), 1244.4(0.2)
4544.4(0.4)	4545.0(11.1), 3740.6(13.9), 2223.0(0.7), 2132.7(3.0), 1925.9(2.6), 1802.8(1.0)
4546.5(0.7)	3151.3(4.3), 2229.2(1.0)
4548.9(0.5)	2762.4(2.4), 1748.6(0.6), 1577.1(0.6), 1479.4(2.8), 1447.1(0.3)
4549.8(0.5)	3746.2(12.5), 3155.1(8.4), 2566.2(2.0), 1836.2(5.2), 1809.3(4.3)
4552.1(0.4)	2234.7(2.1), 2214.6(2.9), 2205.6(2.7), 2091.4(2.2), 1513.5(2.0), 1482.6(0.3)
4553.0(0.4)	2501.4(5.0), 2327.0(5.2), 2230.6(3.9), 2222.2(3.2), 1856.2(1.6), 1422.1(0.9), 1213.4(1.0)
4574.2(0.3)	3179.3(25.0), 3117.2(37.6), 2787.7(14.2), 2591.1(5.9), 2522.8(10.3), 2252.8(7.5), 2243.4(16.7), 2227.6(7.8), 2053.2(2.7), 2044.8(3.4), 1955.9(10.1), 1877.1(9.8), 1860.6(14.0), 1774.1(1.0), 1644.1(8.2), 1618.7(1.7), 1594.7(2.4), 1473.0(0.4), 1461.0(1.2), 1397.1(1.0), 1375.2(0.7), 1194.7(2.1)
4576.4(0.6)	3773.1(7.6), 2525.5(6.9), 2349.7(4.4)
4584.3(1.0)	4584.3(5.2)
4594.6(1.0)	2701.7(0.4)
4597.2(0.4)	3793.8(7.2), 2810.7(13.7), 2613.7(14.6), 2370.7(5.7), 2275.5(3.8), 2076.9(2.9), 1883.8(5.7), 1796.6(1.7), 1591.2(3.5)
4601.8(0.6)	3144.6(2.1), 1904.6(0.9), 1263.0(0.4)
4605.8(0.4)	4605.4(14.7), 2820.0(3.3), 2712.7(1.7), 2623.0(2.4), 2288.0(4.1), 2284.0(3.8), 2268.8(8.7), 2170.9(5.4)
4607.7(1.0)	3212.7(1.7)
4610.0(0.7)	3215.3(6.2), 3152.8(8.2)
4640.6(0.7)	3836.8(21.0), 1927.0(0.6)
4649.0(0.7)	2862.0(3.4), 1936.1(1.6)
4652.9(1.0)	4652.9(6.7)
4660.2(0.5)	3856.8(5.8), 2323.1(1.3), 2199.7(1.8), 1859.4(1.1), 1476.6(0.7)
4665.8(0.5)	3862.7(8.2), 2137.0(2.9), 1626.8(0.9), 1595.7(0.5), 1483.2(0.5)
4668.1(1.0)	2321.5(1.2)
4694.9(0.4)	3237.9(2.7), 2908.8(10.3), 2712.3(1.6), 2283.3(2.2), 1997.1(1.3), 1954.5(2.1), 1738.6(0.9)
4698.0(0.4)	4698.2(9.1), 3241.2(3.8), 2366.8(4.9), 2351.4(1.3), 1956.8(1.7), 1743.0(0.9), 1629.3(0.5), 1585.0(1.7)
4706.1(0.3)	3902.7(24.8), 3311.2(12.3), 2919.5(4.3), 2723.2(1.4), 2479.3(2.4), 2375.4(13.9), 2359.7(1.6), 2009.4(3.5), 1965.7(1.7), 1850.0(0.6), 1776.5(1.1), 1762.7(5.2), 1636.0(0.4), 1603.5(0.3), 1593.4(0.8), 1225.8(2.9)
4712.2(1.0)	4712.2(9.7)
4718.2(0.7)	3323.5(3.8), 2387.1(2.2)
4733.4(0.5)	3929.6(16.0), 2750.2(7.6), 2507.6(5.6), 1932.3(0.3), 1394.5(0.3)
4743.7(0.7)	4743.8(17.3), 2851.0(0.6), 2030.7(1.5), 1674.0(0.4), 1641.4(0.4)
4753.9(0.5)	3949.8(4.1), 3359.0(3.0), 3297.3(11.5), 2967.8(14.2), 1652.0(0.4)
4757.7(0.6)	3954.6(6.8), 3362.5(1.8), 1626.1(0.5)
4759.3(0.5)	3302.8(10.2), 2973.0(4.1), 2776.2(1.1), 1657.0(0.2)
4766.5(0.4)	2980.0(2.3), 2783.9(2.0), 2449.6(1.5), 2429.1(1.4), 2419.5(2.1), 1966.2(0.2), 1426.6(0.2)
4769.6(1.1)	1657.1(2.0)
4785.1(0.6)	2998.8(3.1), 2801.8(2.7), 1716.0(0.3)
4789.4(0.7)	3985.4(3.0), 3332.8(11.5)
4794.0(1.0)	4794.0(6.0)

TABLE I. (*Continued*).

$E_{level}(\Delta E)$	$E_\gamma(I_\gamma)$
4799.2(1.0)	2816.1(1.6)
4803.7(0.5)	4000.2(13.3), 3408.8(6.1), 2820.0(2.3), 2578.2(2.8)
4808.1(0.4)	4004.5(9.8), 3412.9(7.4), 3350.7(2.4), 2825.7(1.2), 2582.0(4.0), 2461.7(2.2), 1706.0(0.2)
4809.1(1.0)	4809.1(3.4)
4835.1(0.4)	4031.0(26.0), 3440.1(3.2), 2851.5(13.0), 2514.0(2.6), 2035.0(0.3), 1879.6(0.9), 1651.2(0.8)
4849.5(0.7)	3454.8(3.7), 3392.3(1.6)
4870.2(1.0)	4066.6(2.4)
4872.6(0.8)	2541.6(2.6), 2175.9(1.1)
4881.5(0.7)	4077.7(2.1), 3424.8(1.5)
4883.1(1.0)	4883.1(7.1)
4901.1(0.5)	3114.2(5.5), 2918.5(6.8), 2564.2(2.1), 2554.5(0.8)
4909.6(1.0)	4106.0(1.9)
4937.6(1.0)	4134.0(2.2)
4949.2(0.5)	4145.7(1.5), 3492.9(1.0), 2966.2(5.9), 2761.9(0.4)
4956.3(1.0)	3499.4(1.8)
4972.7(1.0)	3186.4(2.5)
4995.4(0.6)	4191.5(9.4), 2658.4(0.8), 2298.6(0.8)
5000.6(1.0)	5000.6(7.7)
5005.8(1.0)	4202.2(1.3)
5010.5(0.7)	4207.5(2.2), 3026.8(2.8)
5031.5(1.0)	5031.5(1.5)
5032.8(1.0)	3049.6(2.5)
5035.2(1.0)	4231.6(1.0)
5067.6(1.0)	4264.0(1.3)
5076.7(1.0)	4273.1(2.2)
5088.5(0.6)	4284.7(2.2), 3693.7(2.5), 3631.7(2.2)
5098.4(1.0)	4294.8(2.1)
5106.2(1.0)	4302.6(3.0)
5110.6(1.0)	4307.0(2.0)
5128.9(1.0)	4325.3(1.5)
5142.7(0.7)	3748.0(2.8), 2445.5(1.0)
5165.5(0.7)	3770.1(2.3), 3709.0(1.4)
5176.1(1.0)	4372.5(1.4)
5181.0(1.0)	4377.4(6.2)
5193.6(1.0)	4390.0(2.3)
5207.6(1.0)	4404.0(1.3)
5211.2(1.0)	4407.6(1.5)
5218.6(0.7)	4415.6(2.8), 3823.0(1.5)
5224.9(1.0)	3830.0(2.2)
5246.6(1.0)	4443.0(0.6)
5250.3(0.6)	4447.0(2.8), 3855.7(1.3), 3792.7(0.6)
5251.6(1.0)	3856.6(2.1)
5254.5(0.6)	4450.2(2.8), 3859.9(1.0), 3798.0(1.2)
5296.0(0.7)	4492.5(1.0), 3839.0(0.5)
5327.5(1.0)	4523.8(0.7)
5334.0(1.0)	4530.4(1.0)
5353.1(1.0)	3896.2(0.9)
5359.6(1.0)	3466.6(0.6)
5414.6(1.0)	4611.0(0.6)
5450.7(1.0)	4647.1(0.6)
5661.8(1.0)	4858.2(0.9)
5725.4(1.0)	4921.8(0.7)
5880.3(1.0)	5076.7(0.4)
5887.8(1.0)	5084.2(0.3)

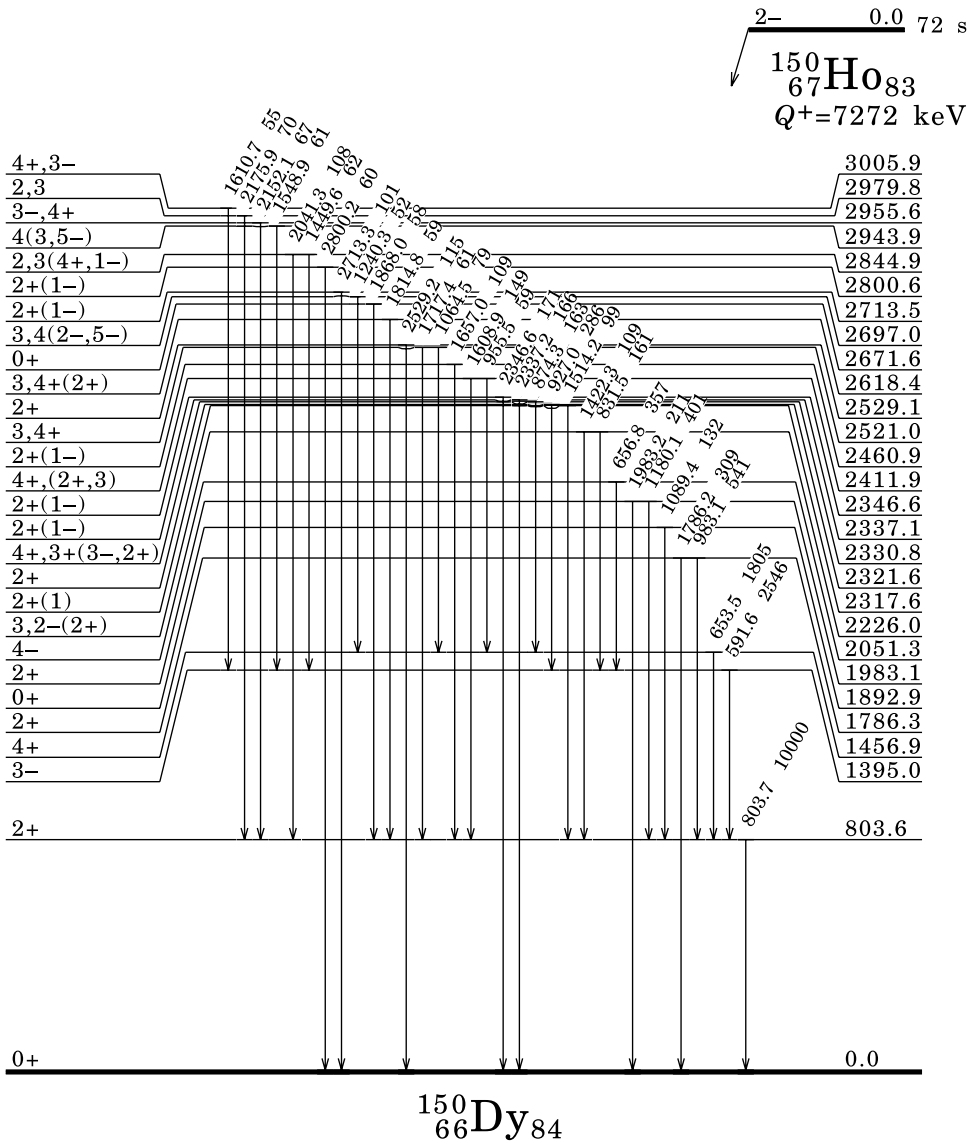

FIG. 5. Partial level scheme, lower part. Only transitions with intensities larger than 50 units, relative to $I=10\,000$ units of the 803-keV transition or equivalently 12 514 parent decays, are presented. Figures 5 and 6 together include only one-sixth of all levels and only 1/20 of all γ rays observed in the present experiment.

and their uncertainties were obtained using a program [9] which optimizes level energies using as input information all the γ cascades defining each level. A simplified version of the level scheme is presented in Figs. 5 and 6 where only γ transitions with intensities larger than 50 units relative to the 803-keV transition with $I=10\,000$ units are presented (this represents 40 units per 10^4 ^{150}Ho 2^- β decays). The purpose of the simplified picture is to give an impression of the strongest lines in the decay and their location in the level scheme. The complete level scheme is documented in Table I.

In total we have observed 1064 γ lines and 295 levels in ^{150}Dy. Due to the complexity of the level scheme the intensity of most of the lines is determined from a combination of the analysis of gated spectra and singles. The observed, very strong β feeding to a narrow interval near 4.4 MeV is in accord with our first-order expectation and with the observation using the total absorption technique [5]. The decay pattern of the levels is quite complex. See, for instance, the level at 4421-keV excitation, one of the most strongly populated states, which decays by 34 observed γ decay branches.

Due to the large number of observed γ transitions, the assumption of GT character of the β decay ($\Delta\pi=0,\Delta J=0,\pm1$), and the transitions observed to low-lying levels of known J^π [10], it was possible to assign spins and parities unambiguously to many of the ^{150}Dy levels at high excitation energy. Also used in the following discussion are the levels at 2187-keV excitation assigned 5^- and the level at 2051 keV assigned 4^-. The assignments of J^π to these levels were based on the similarity in the γ decay to the ^{148}Gd case. However, the J^π was further confirmed by many possible cross-checks from other linking transitions. These results are summarized in Table II, where the direct β feeding to each level is also quoted [for the calculation of the $\log_{10} ft$ in Table II the $Q_{EC}=7372(27)$ keV [11] and $T_{1/2}$

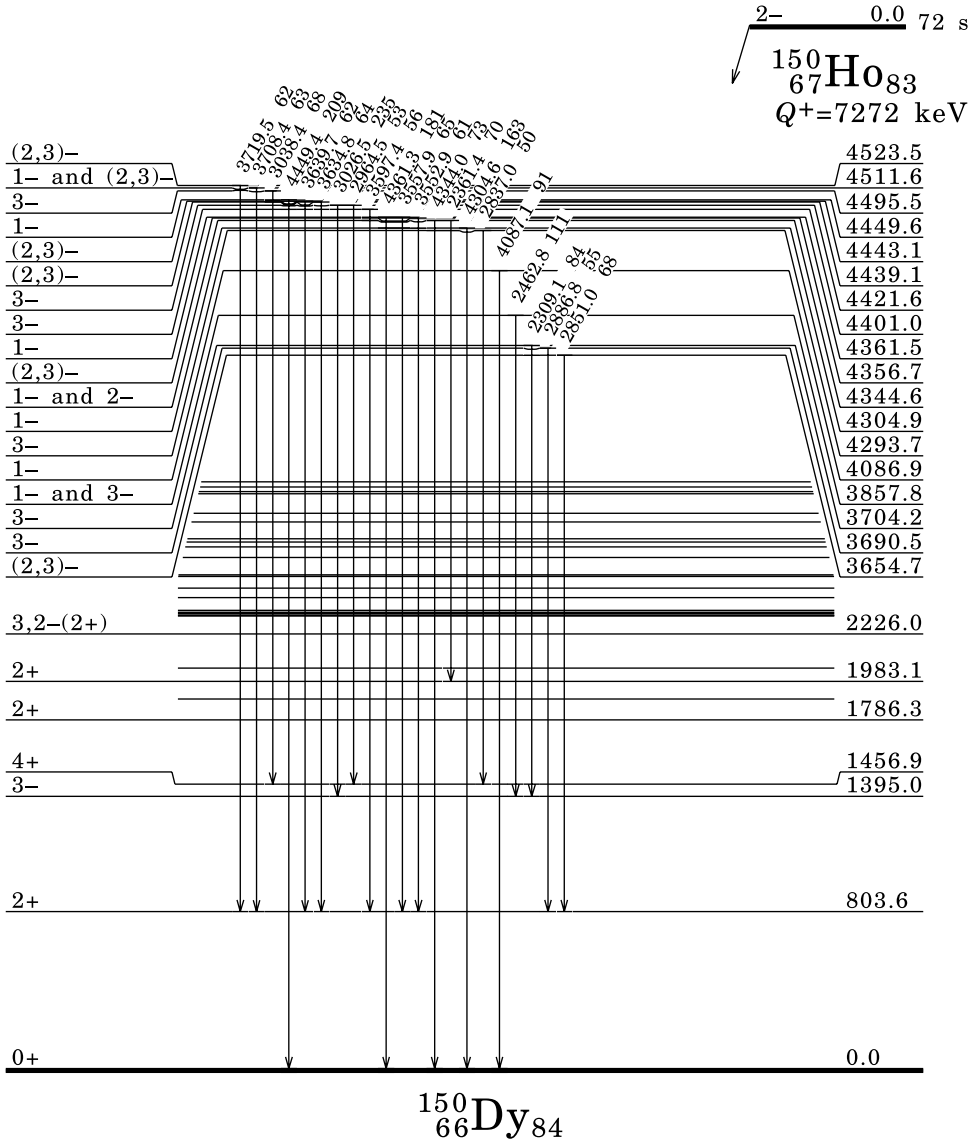

FIG. 6. Partial level scheme, upper part. Only transitions with intensities larger than 50 units, relative to $I=10\,000$ units of the 803-keV transition or equivalently 12 514 parent decays, are presented. Figures 5 and 6 together include only one-sixth of all levels and only 1/20 of all γ rays observed in the present experiment.

$=72(4)$ s [10] values were used]. The criteria for assigning spins and parities to the levels were the following. First of all the data define an energy interval in which only direct β^+/EC feeding, but no γ feeding, from higher-lying states was observed. The definition of the direct β-feeding interval is important for the correct application of the GT selection rules for allowed decay. This energy range is located between 3.6 and 5.9 MeV excitation energy, but conservatively we have considered it to be between 3.8 and 5.9 MeV. Its position was also supported by comparison with the total absorption spectrometer (TAS) results (see Fig. 7) [2,5]. Once this interval is defined we had two sets of criteria for the assignment of spin parity to the levels in the interval which we call strong and weak arguments. The first strong argument corresponds to the assignment of 1^- to a level which decays (mainly) to the ^{150}Dy 0^+ ground state. The second strong argument corresponds to the assignment of 3^- to a level which decays to the 4^+ state (1457 keV) or (and) to the 5^- state (2186 keV). Contrary to the 1^- and 3^- cases the 2^- assignment is less straightforward. Weak assignment arguments are given as follows.

(a) If the level does not decay to the ground state, it is unlikely that it is a 1^- state, thus other possibilities were considered.

(b) If the dominant deexcitation transition goes to the 2^+ state, the level is probably neither 1^- nor 3^-, but the 3^- is not completely excluded. These levels were assigned $(2,3)^-$ if they decay mainly to 2^+ states and $(3,2)^-$ if they decay to 2^+ states but this is not the main decay mode.

(c) If the dominant or a very strong transition populates the 4^- state (2051 keV), then the level was assigned 3^-. The validity of these criteria is generally supported by the results of our shell-model calculation (the following section) and by the absence of inconsistencies in the connecting transitions

TABLE II. Levels observed in this work (in keV) with their assigned J^π. The total β feeding is normalized to 10^4 parent decays. The feeding to the ground state is assumed here to be 0.

E_{level}	J^π	β feeding	$\log_{10} ft$	E_{level}	J^π	β feeding	$\log_{10} ft$
0.0	0^+			2697.0	3, $4(2^-,5^-)$	17.6	7.44
803.6	2^+	1287.3	6.28	2713.6	$2^+(1^-)$	40.3	7.07
1395.0	3^-	157.4	6.99	2740.8	$3^-(2^+)$	31.2	7.17
1456.9	4^+	487.6	6.48	2800.6	$2^+(1^-)$	64.7	6.82
1786.3	2^+	272.4	6.61	2836.5		29.1	7.16
1893.0	0^+	21.2	7.68	2844.9	2, $3(4^+,1^+)$	110.6	6.57
1983.1	2^+	163.6	6.76	2855.8	$3(2^+,4^+)$	47.2	6.94
2051.2	4^-	77.4	7.06	2910.9	(4, 5, 6)	1.1	8.54
2186.8	5^-	28.3	7.44	2928.2		4.5	7.93
2226.0	3, $2^-(2^+)$	1.9	8.61	2930.3	$4(3^-)$	0.3	9.08
2253.7	0^+, 1, 2, (3^-)	10.5	7.84	2943.9	$4(3,5^-)$	9.3	7.61
2317.6	$2^+(1)$	48.2	7.16	2946.8	(3, 4, 5)	3.4	8.05
2321.6	2^+	128.9	6.73	2955.6	$3^-,4^+$	73.3	6.71
2330.8	$4^+,3^+(3^-,2^+)$	29.8	7.36	2972.0	$2^+(1^-)$	40.0	6.97
2337.0	$2^+(1^-)$	79.0	6.93	2979.8	2, 3	31.1	7.07
2346.6	$2^+(1^-)$	123.6	6.74	3005.9	$4^+,3^-$	48.2	6.87
2411.9	4^+ $(2^+,3)$	46.0	7.14	3010.4	0^+, 1, 2, (3^-)	1.4	8.41
2419.0	3^-, 4, 5^-	21.2	7.47	3038.6	$2^+(1^-)$	49.6	6.84
2434.8	1^-, 2	23.1	7.43	3067.9	2, 3, $4(1^-)$	2.1	8.20
2460.9	$2^+(1^-)$	93.1	6.81	3069.2	$1(2^+)$	11.8	7.45
2509.7		3.2	8.25	3082.8	(3, 4, 5)	2.1	8.19
2521.0	3, 4^+	83.0	6.84	3101.8	$2(1^-,3^-)$	26.2	7.09
2529.1	2^+	85.6	6.82	3107.9	(3, 4, 5)	1.7	8.27
2618.4	3, $4^+(2^+)$	28.0	7.27	3112.5	$3(2^+,4^+)$	27.6	7.06
2635.3	2, 3, 4	4.7	8.04	3131.4	2, $3(4^+,1^-)$	24.2	7.11
2671.6	0^+	9.9	7.70	3133.8	(3, 4, 5)	2.4	8.11
3141.0	0^+, 1, 2, $3(4^+)$	3.2	7.98	3414.3	(3, 4)	3.9	7.77
3150.4	$4(3^-,5^-)$	24.6	7.10	3422.6	(1, 2, 3)	5.9	7.60
3151.9	$3(2^+,4^+)$	13.5	7.35	3440.6	(1, 2, 3)	6.6	7.54
3156.4	$3(4^+)$	28.9	7.02	3441.0	(3, 4, 5)	5.0	7.66
3172.7	(2, 3)	42.1	6.85	3458.7	$3^-,4^+$	17.4	7.11
3177.2	$4^+(3^-)$	33.7	6.95	3464.5	(2, 3, 4)	2.1	8.03
3183.3	$2^-,3^-$	24.5	7.08	3465.2	(2, 3, 4)	4.0	7.75
3194.3	$(0^+$, 1, 2, 3)	3.1	7.98	3466.9	(3, 4, 5)	2.3	8.00
3197.6	(2, 3)	1.3	8.36	3473.7	(2, 3, 4)	2.7	7.92
3199.0	(3, 4)	11.5	7.41	3480.5	(2, 3)	5.8	7.58
3257.9	(2, 3, 4)	13.7	7.31	3496.1	$(0^+$, 1, 2, 3)	6.3	7.54
3279.2	2^+, (1^-)	14.4	7.28	3497.0	(2, 3, 4, 0^+)	5.0	7.64
3292.3	(3)	30.0	6.95	3500.6	(2, 3)	17.6	7.09
3294.2	(4)	9.3	7.46	3528.6	3 (4^-)	14.2	7.17
3304.8	(3, 4)	39.6	6.82	3529.4	(2, 3, 1, 0^+)	15.1	7.14
3326.4	$(0^+$, 1, 2, 3)	1.3	8.30	3530.3	(1, 2, 3)	3.5	7.78
3335.4	1, 2^+	7.6	7.53	3535.7	$(2,3)^-$	43.3	6.68
3339.5	$2^+(1^-)$	34.0	6.87	3542.2	$(0^+$, 1, 2, 3)	1.0	8.33
3348.8	(3, 4, 5)	9.2	7.44	3550.2	(2, 3, 4)	8.0	7.41
3356.3	(3)	17.7	7.15	3565.0	(2, 3, 4)	4.0	7.70
3366.2	(2, 3, 4)	3.8	7.81	3567.5	3^-	38.6	6.71
3378.8	3^-	12.6	7.28	3577.7	$(0^+$, 1, 2, 3)	7.6	7.41
3383.1	(3)	16.2	7.17	3586.1	(3, 4, 5)	3.3	7.77
3394.9	(3, 4, 5)	4.7	7.71	3588.9	(1^-) and (3^-)	37.8	6.71
3405.1	(3, 4)	7.8	7.48	3600.6	(3, 4)	3.5	7.75
3412.9	(3, 4, 5)	2.3	8.00	3613.1	(3, 4, 5)	2.2	7.94

TABLE II. (*Continued*).

E_{level}	J^{π}	β feeding	$\log_{10} ft$	E_{level}	J^{π}	β feeding	$\log_{10} ft$
3638.6	(3, 4)	3.7	7.70	3926.9	$(2,3)^-$	13.4	7.01
3654.6	$(2,3)^-$	58.7	6.50	3929.8	$(2,3)^-$	4.0	7.53
3660.3	(3, 4)	18.0	7.01	3968.4	3^-	21.1	6.80
3690.5	3^-	64.3	6.44	3980.9	3^-	2.1	7.79
3693.4		1.8	8.00	4000.3	$(3,2)^-$	13.4	6.98
3704.2	3^-	140.9	6.09	4009.3	1^-	1.0	8.08
3724.0	(2, 3, 4)	4.7	7.55	4045.8	$(2,3)^-$	48.5	6.39
3733.1	3^-	56.7	6.47	4052.6	$(2,3)^-$	1.1	8.03
3743.5	(3, 4, 5)	2.7	7.78	4086.8	1^-	102.4	6.05
3749.7	(1, 2, 3)	13.4	7.09	4099.9	1^-	32.4	6.55
3766.6	(2, 3, 4)	10.6	7.18	4102.3	1^- and $(2,3)^-$	89.8	6.10
3782.8	(2, 3, 4)	3.2	7.70	4116.6	$(2,3)^-$	11.3	7.00
3789.1	$(0^+, 1, 2, 3)$	7.0	7.36	4118.8	$(3,2)^-$	6.7	7.22
3792.6	$2^+,1^-$	41.9	6.58	4129.1	$(2,3)^-$	13.4	6.92
3804.1	2^+	27.8	6.75	4151.5	$(3,2)^-$	3.7	7.47
3812.8	3^-	6.0	7.41	4154.0	$(2,3)^-$	11.1	6.99
3834.2	1^-	10.8	7.15	4162.7	3^-	11.6	6.97
3857.8	1^- and 3^-	199.9	5.87	4170.6	3^- and 1^-	12.2	6.94
3870.0	3^-	19.8	6.87	4196.6	$(2,3)^-$	8.1	7.10
3873.5	$(2,3)^-$	32.1	6.66	4199.0	1^-	3.8	7.44
3892.2	$(3,2)^-$	2.9	7.70	4208.4	$(2,3)^-$	1.6	7.80
3895.6	1^-	34.4	6.62	4216.3	$(3,2)^-$	1.6	7.80
3900.8	3^-	4.4	7.51	4220.6	3^-	22.3	6.65
3903.7	$(3,2)^-$	4.2	7.53	4224.3	$(3,2)^-$	5.2	7.29
3916.0	3^-	62.9	6.35	4233.8	1^-	3.2	7.49
3924.2	3^-	80.0	6.24	4253.5	$(3,2)^-$	5.1	7.28
4255.4	1^-	4.2	7.36	4445.8	3^-	100.9	5.90
4264.5	$(2,3)^-$	10.1	6.97	4449.6	1^-	203.0	5.59
4270.3	$(2,3)^-$	4.9	7.29	4460.6	$(3)^-$	14.2	6.74
4278.4	3^-	1.8	7.73	4469.6	$(2,3)^-$	15.1	6.71
4293.7	3^-	63.3	6.17	4480.5	1^-	18.8	6.61
4304.9	1^-	148.8	5.79	4482.6	3^-	74.0	6.01
4311.4	$(2,3)^-$	1.0	7.94	4486.6	$(3)^-$	64.1	6.07
4322.0	$(2,3)^-$	26.7	6.53	4487.8	1^-	7.5	7.01
4340.2	$(2,3)^-$	1.0	7.97	4491.7	3^-	224.1	5.53
4342.3	1^-	25.8	6.54	4495.5	3^-	282.9	5.43
4344.6	1^- and $(2,3)^-$	310.7	5.46	4511.6	1^- and $(2,3)^-$	72.9	6.01
4355.2	1^-	5.0	7.25	4518.4	1^-	30.5	6.38
4356.6	$(2,3)^-$	127.8	5.84	4519.5	$(3,2)^-$	4.4	7.22
4361.5	1^-	214.4	5.61	4521.6	3^-	26.5	6.44
4373.4	$(3)^-$	19.6	6.65	4523.5	$(2,3)^-$	61.3	6.08
4377.4	1^-	27.9	6.49	4544.4	1^- and 3^-	26.0	6.44
4389.6	$(2,3)^-$	9.2	6.97	4546.5	$(3,2)^-$	4.3	7.23
4401.0	3^-	199.1	5.62	4548.9	$(2,3)^-$	5.4	7.12
4417.1	$(2,3)^-$	41.3	6.30	4549.8	$(2,3)^-$	26.1	6.44
4421.6	3^-	400.2	5.31	4552.1	$(2,3)^-$	9.8	6.86
4427.0	$(3,2)^-$	68.2	6.08	4553.0	$(3)^-$	16.7	6.63
4429.1	$(3,2)^-$	2.6	7.50	4574.2	3^-	147.9	5.68
4431.6	1^-	23.3	6.54	4576.4	$(3)^-$	15.2	6.66
4439.1	$(2,3)^-$	72.0	6.05	4584.3	1^-	4.2	7.22
4443.1	$(2,3)^-$	93.5	5.93	4594.6	1^-	0.3	8.33
4444.2	1^-	7.0	7.06	4597.2	$(2,3)^-$	47.3	6.16

TABLE II. (*Continued*).

E_{level}	J^{π}	β feeding	$\log_{10} ft$	E_{level}	J^{π}	β feeding	$\log_{10} ft$
4601.8	3^-	2.7	7.40	4803.7	$(2,3)^-$	19.7	6.44
4605.8	1^-	35.5	6.28	4808.1	3^-	21.9	6.39
4607.7	$(3,2)^-$	1.4	7.69	4809.1	1^-	2.7	7.30
4610.0	3^-	11.6	6.76	4835.1	$(2,3)^-$	37.7	6.15
4640.6	$(2,3)^-$	17.4	6.57	4849.5	3^-	4.3	7.09
4649.0	$(2,3)^-$	4.0	7.20	4870.2	$(2,3)^-$	1.9	7.42
4652.9	1^-	5.4	7.08	4872.6	$(2,3)^-$	3.0	7.23
4660.2	$(2,3)^-$	8.6	6.87	4881.5	3^-	2.9	7.24
4665.8	$(2,3)^-$	10.5	6.78	4883.1	1^-	5.7	6.94
4668.1	$(2,3)^-$	1.0	7.81	4901.1	$(2,3)^-$	12.2	6.61
4694.9	3^-	17.0	6.56	4909.6	$(2,3)^-$	1.5	7.50
4698.0	1^- and 3^-	19.2	6.50	4937.6	$(2,3)^-$	1.8	7.43
4706.1	$(2,3)^-$	62.1	5.99	4949.2	3^-	7.1	6.82
4712.2	1^-	7.8	6.88	4956.3	3^-	1.4	7.50
4718.2	$(3,2)^-$	4.8	7.09	4972.7	$(2,3)^-$	2.0	7.35
4733.4	$(2,3)^-$	24.0	6.39	4995.4	$(2,3)^-$	8.9	6.70
4743.7	1^-	16.3	6.55	5000.6	1^-	6.2	6.85
4753.9	3^-	26.7	6.33	5005.8	$(2,3)^-$	1.0	7.62
4757.7	$(2,3)^-$	7.3	6.89	5010.5	$(2,3)^-$	4.0	7.04
4759.3	3^-	12.6	6.65	5031.5	1^-	1.2	7.55
4766.5	$(2,3)^-$	7.8	6.86	5032.8	$(2,3)^-$	2.0	7.33
4769.6	$(3,2)^-$	1.6	7.54	5035.2	$(2,3)^-$	0.8	7.73
4785.1	$(2,3)^-$	4.9	7.05	5067.6	$(2,3)^-$	1.0	7.60
4789.4	3^-	11.7	6.67	5076.7	$(2,3)^-$	1.8	7.37
4794.0	1^-	4.8	7.05	5088.5	3^-	5.6	6.86
4799.2	$(2,3)^-$	1.3	7.63	5098.4	$(2,3)^-$	1.7	7.38
5106.2	$(2,3)^-$	2.4	7.22	5251.6	$(3,2)^-$	1.7	7.30
5110.6	$(2,3)^-$	1.6	7.39	5254.5	3^-	4.0	6.92
5128.9	$(2,3)^-$	1.2	7.51	5296.0	3^-	1.2	7.42
5142.7	$(3,2)^-$	3.1	7.10	5327.5	$(2,3)^-$	0.6	7.74
5165.5	3^-	3.0	7.10	5334.0	$(2,3)^-$	0.8	7.58
5176.1	$(2,3)^-$	1.1	7.51	5353.1	3^-	0.7	7.62
5181.0	$(2,3)^-$	5.0	6.86	5359.6	1^-	0.5	7.79
5193.6	$(2,3)^-$	1.9	7.29	5414.6	$(2,3)^-$	0.5	7.76
5207.6	$(2,3)^-$	1.0	7.53	5450.7	$(2,3)^-$	0.5	7.74
5211.2	$(2,3)^-$	1.2	7.47	5661.8	$(2,3)^-$	0.7	7.46
5218.6	$(2,3)^-$	3.5	7.00	5725.4	$(2,3)^-$	0.6	7.53
5224.9	$(3,2)^-$	1.8	7.29	5880.3	$(2,3)^-$	0.3	7.69
5246.6	$(2,3)^-$	0.5	7.85	5887.8	$(2,3)^-$	0.2	7.81
5250.3	3^-	3.8	6.95				

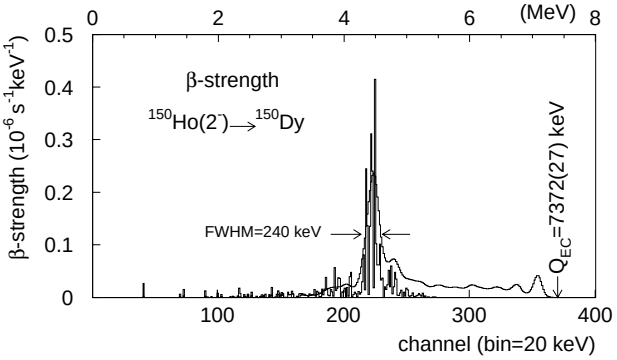

FIG. 7. Results of the CLUSTER CUBE experiment (solid line) together with the TAS data (dashed line) [5,6].

to other levels with assigned spin parity. For levels below 3.8 MeV, the GT selection rules cannot be strictly applied. Their spin-parity assignment was based on γ transitions connecting them to levels of known or newly assigned spin parity. In our discussion of the structure below, we will not consider these levels at lower excitation energy but only the higher excitation states related to the resonance. We plan to report on a more detailed discussion of the ^{150}Dy low-lying states after completion of the analysis of similar data for the ^{150}Ho 9^+ decay.

The large amount of spectroscopic data obtained in this experiment reveals new features in the decay of the ^{150}Ho 2^- isomer. Figure 7 shows our results compared with those obtained using the TAS technique in terms of strength. Both

TABLE III. Two-body matrix elements used in the shell-model calculations. All matrix elements are taken from experiment with the exception of the $\langle \pi\pi|V|\pi\pi\rangle_{0^+}$ matrix elements (see text for details). The $\langle \pi\pi|V|\pi\pi\rangle$ matrix elements are deduced from ^{148}Dy. The $\langle \pi\nu|V|\pi\nu\rangle$ elements are deduced from ^{148}Tb and the $\langle \nu\nu|V|\nu\nu\rangle$ matrix elements from ^{148}Gd (see the Appendix).

Matrix element	Intensity (keV)	Matrix element	Intensity (keV)
$\langle \pi h^2_{11/2}\|V\|\pi h^2_{11/2}\rangle_{0^+}$	−1607	$\langle \pi h_{11/2}\nu h_{9/2}\|V\|\pi h_{11/2}\nu h_{9/2}\rangle_{1^+}$	−1349
$\langle \pi h^2_{11/2}\|V\|\pi h^2_{11/2}\rangle_{2^+}$	−865	$\langle \pi h_{11/2}\nu h_{9/2}\|V\|\pi h_{11/2}\nu h_{9/2}\rangle_{2^+}$	−839
$\langle \pi h^2_{11/2}\|V\|\pi h^2_{11/2}\rangle_{4^+}$	−115	$\langle \pi h_{11/2}\nu h_{9/2}\|V\|\pi h_{11/2}\nu h_{9/2}\rangle_{3^+}$	−399
$\langle \pi h^2_{11/2}\|V\|\pi h^2_{11/2}\rangle_{6^+}$	189	$\langle \pi h_{11/2}\nu h_{9/2}\|V\|\pi h_{11/2}\nu h_{9/2}\rangle_{4^+}$	−419
$\langle \pi h^2_{11/2}\|V\|\pi h^2_{11/2}\rangle_{8^+}$	290	$\langle \pi h_{11/2}\nu h_{9/2}\|V\|\pi h_{11/2}\nu h_{9/2}\rangle_{5^+}$	−299
$\langle \pi h^2_{11/2}\|V\|\pi h^2_{11/2}\rangle_{10^+}$	377	$\langle \pi h_{11/2}\nu h_{9/2}\|V\|\pi h_{11/2}\nu h_{9/2}\rangle_{6^+}$	−359
$\langle \pi h^2_{11/2}\|V\|\pi d^2_{3/2}\rangle_{0^+}$	1159	$\langle \pi h_{11/2}\nu h_{9/2}\|V\|\pi h_{11/2}\nu h_{9/2}\rangle_{7^+}$	−279
$\langle \pi h_{11/2}\pi d_{3/2}\|V\|\pi h_{11/2}\pi d_{3/2}\rangle_{4^-}$	251	$\langle \pi h_{11/2}\nu h_{9/2}\|V\|\pi h_{11/2}\nu h_{9/2}\rangle_{8^+}$	−315
$\langle \pi h_{11/2}\pi d_{3/2}\|V\|\pi h_{11/2}\pi d_{3/2}\rangle_{5^-}$	428	$\langle \pi h_{11/2}\nu h_{9/2}\|V\|\pi h_{11/2}\nu h_{9/2}\rangle_{9^+}$	−246
$\langle \pi h_{11/2}\pi d_{3/2}\|V\|\pi h_{11/2}\pi d_{3/2}\rangle_{6^-}$	579	$\langle \pi h_{11/2}\nu h_{9/2}\|V\|\pi h_{11/2}\nu h_{9/2}\rangle_{10^+}$	−485
$\langle \pi h_{11/2}\pi d_{3/2}\|V\|\pi h_{11/2}\pi d_{3/2}\rangle_{7^-}$	−5	$\langle \pi d^2_{3/2}\|V\|\pi d^2_{3/2}\rangle_{0^+}$	−269
$\langle \pi h^2_{11/2}\|V\|\pi s^2_{1/2}\rangle_{0^+}$	819	$\langle \pi d^2_{3/2}\|V\|\pi d^2_{3/2}\rangle_{2^+}$	200
$\langle \pi h_{11/2}\pi s_{1/2}\|V\|\pi h_{11/2}\pi s_{1/2}\rangle_{5^-}$	−141	$\langle \pi d^2_{3/2}\|V\|\pi s^2_{1/2}\rangle_{0^+}$	−473
$\langle \pi h_{11/2}\pi s_{1/2}\|V\|\pi h_{11/2}\pi s_{1/2}\rangle_{6^-}$	363	$\langle \pi d_{3/2}\pi s_{1/2}\|V\|\pi d_{3/2}\pi s_{1/2}\rangle_{1^+}$	400
$\langle \pi h_{11/2}\nu f_{7/2}\|V\|\pi h_{11/2}\nu f_{7/2}\rangle_{2^+}$	−394	$\langle \pi d_{3/2}\pi s_{1/2}\|V\|\pi d_{3/2}\pi s_{1/2}\rangle_{2^+}$	0
$\langle \pi h_{11/2}\nu f_{7/2}\|V\|\pi h_{11/2}\nu f_{7/2}\rangle_{3^+}$	−291	$\langle \pi d_{3/2}\nu f_{7/2}\|V\|\pi d_{3/2}\nu f_{7/2}\rangle_{2^-}$	−774
$\langle \pi h_{11/2}\nu f_{7/2}\|V\|\pi h_{11/2}\nu f_{7/2}\rangle_{4^+}$	−197	$\langle \pi d_{3/2}\nu f_{7/2}\|V\|\pi d_{3/2}\nu f_{7/2}\rangle_{3^-}$	−59
$\langle \pi h_{11/2}\nu f_{7/2}\|V\|\pi h_{11/2}\nu f_{7/2}\rangle_{5^+}$	−221	$\langle \pi d_{3/2}\nu f_{7/2}\|V\|\pi d_{3/2}\nu f_{7/2}\rangle_{4^-}$	−177
$\langle \pi h_{11/2}\nu f_{7/2}\|V\|\pi h_{11/2}\nu f_{7/2}\rangle_{6^+}$	−146	$\langle \pi d_{3/2}\nu f_{7/2}\|V\|\pi d_{3/2}\nu f_{7/2}\rangle_{5^-}$	−429
$\langle \pi h_{11/2}\nu f_{7/2}\|V\|\pi h_{11/2}\nu f_{7/2}\rangle_{7^+}$	−244	$\langle \pi d_{3/2}\nu h_{9/2}\|V\|\pi d_{3/2}\nu h_{9/2}\rangle_{3^-}$	−200
$\langle \pi h_{11/2}\nu f_{7/2}\|V\|\pi h_{11/2}\nu f_{7/2}\rangle_{8^+}$	−166	$\langle \pi d_{3/2}\nu h_{9/2}\|V\|\pi d_{3/2}\nu h_{9/2}\rangle_{4^-}$	−100
$\langle \pi h_{11/2}\nu f_{7/2}\|V\|\pi h_{11/2}\nu f_{7/2}\rangle_{9^+}$	−482	$\langle \pi d_{3/2}\nu h_{9/2}\|V\|\pi d_{3/2}\nu h_{9/2}\rangle_{5^-}$	0
		$\langle \pi d_{3/2}\nu h_{9/2}\|V\|\pi d_{3/2}\nu h_{9/2}\rangle_{6^-}$	−300
$\langle \pi s^2_{1/2}\|V\|\pi s^2_{1/2}\rangle_{0^+}$	66	$\langle \nu f_{7/2}\nu h_{9/2}\|V\|\nu f_{7/2}\nu h_{9/2}\rangle_{1^+}$	−189
$\langle \pi s_{1/2}\nu f_{7/2}\|V\|\pi s_{1/2}\nu f_{7/2}\rangle_{3^-}$	−326	$\langle \nu f_{7/2}\nu h_{9/2}\|V\|\nu f_{7/2}\nu h_{9/2}\rangle_{2^+}$	−293
$\langle \pi s_{1/2}\nu f_{7/2}\|V\|\pi s_{1/2}\nu f_{7/2}\rangle_{4^-}$	−411	$\langle \nu f_{7/2}\nu h_{9/2}\|V\|\nu f_{7/2}\nu h_{9/2}\rangle_{3^+}$	−169
$\langle \nu f^2_{7/2}\|V\|\nu f^2_{7/2}\rangle_{0^+}$	−1642	$\langle \nu f_{7/2}\nu h_{9/2}\|V\|\nu f_{7/2}\nu h_{9/2}\rangle_{4^+}$	−200
$\langle \nu f^2_{7/2}\|V\|\nu f^2_{7/2}\rangle_{2^+}$	−858	$\langle \nu f_{7/2}\nu h_{9/2}\|V\|\nu f_{7/2}\nu h_{9/2}\rangle_{5^+}$	−179
$\langle \nu f^2_{7/2}\|V\|\nu f^2_{7/2}\rangle_{4^+}$	−226	$\langle \nu f_{7/2}\nu h_{9/2}\|V\|\nu f_{7/2}\nu h_{9/2}\rangle_{6^+}$	−256
$\langle \nu f^2_{7/2}\|V\|\nu f^2_{7/2}\rangle_{6^+}$	169	$\langle \nu f_{7/2}\nu h_{9/2}\|V\|\nu f_{7/2}\nu h_{9/2}\rangle_{7^+}$	−170
		$\langle \nu f_{7/2}\nu h_{9/2}\|V\|\nu f_{7/2}\nu h_{9/2}\rangle_{8^+}$	−345

techniques consistently reveal the existence of an intense resonance at 4.4 MeV excitation energy.

IV. THEORETICAL INTERPRETATION

In order to investigate the excitation energies of the 1^-, 2^-, and 3^- states of the $\pi h_{11/2}\pi d_{3/2}\nu h_{9/2}\nu f_{7/2}$ four-particle configuration in the daughter nucleus a shell-model calculation based on experimental two-body interaction energies was carried out.

The calculation was performed in a restricted configuration space, with two protons in the $s_{1/2}$, $d_{3/2}$, and $h_{11/2}$ and two neutrons in the $f_{7/2}$ and $h_{9/2}$ orbitals. In general only diagonal elements for the six, two-body interactions needed for the four-particle configuration were used. One important feature in this calculation is that all effective, two-body interactions were extracted from the observed excitation energies of the two-body multiplet members in the respective two-nucleon nuclei ^{148}Dy, ^{148}Tb, and ^{148}Gd ([12–15] and references therein), except for the $\pi\ d_{3/2}\nu h_{9/2}$ quartet [16], which so far has not been identified in ^{148}Tb. All input data are compiled in Table III and explained in the Appendix, except for $\pi\ d_{3/2}\nu h_{9/2}$, which is estimated theoretically [16]. A special treatment was given to the six matrix elements corresponding to the $h^2_{11/2}$, $d^2_{3/2}$, and $s^2_{1/2}$ configurations coupled to 0^+. In this case diagonal and nondiagonal elements were considered. This was needed for a proper treatment of pairing. The matrix elements were taken to be proportional to $[(2J_1+1)(2J_2+1)]^{1/2}(-1)^{l_1+l_2+1}(J_{1,2}=11/2,3/2,1/2;\ l_{1,2}=5,2,0)$. The overall strength was fixed to reproduce the known 1678 keV, 0^+ to 2^+ relative energy in ^{148}Dy. These elements are also given in Table III and are of vital importance for the calculation of the ^{150}Dy 0^+ and ^{150}Ho 2^- ground states (see below). The single-particle energies used in the calculations were $\pi s_{1/2}=0.0$ keV, $\pi h_{11/2}=51.0$ keV, $\pi d_{3/2}=253.0$ keV, $\nu f_{7/2}=0.0$ keV, and $\nu h_{9/2}=1397.0$ keV, as observed in the ^{147}Tb and ^{147}Gd single-particle nuclei. Excitation energies are the result of adding an

TABLE IV. Comparison of the experimental results with the shell-model predictions. The experimental energies and strengths were calculated from the CLUSTER CUBE data by using all observed states between 3.5 and 5.9 MeV with the J^π assignment given in Table II, and weighted with the corresponding strength.

	Energy (keV)		Strength ($g_A^2/4\pi$ units)		
J^π	Expt.	Calc.	Expt.	Expt.$_{norm}$	Calc.
1^-	4380	4326	0.054	0.62	0.67
2^-	4488	4521	0.067	0.77	0.73
3^-	4385	4460	0.120	1.37	1.36
Total			0.241	2.76	2.76

overall term of 5362 keV to the absolute energies obtained in the diagonalization. This term takes into account the ground state masses of the nuclei involved and it is explained in the Appendix. The ^{150}Dy ground state energy obtained in this way was 13 keV, far more accurate than the ± 134-keV error of the calculation originating from the experimental errors of the masses of the seven nuclei contributing to the configuration.

The $\pi h_{11/2}\nu h_{9/2}\pi d_{3/2}\nu f_{7/2}$ configuration populated in the ^{150}Ho 2^- GT decay has altogether 280 levels with spins from 0^- to 15^- between 4.3- and 6.7-MeV excitation, among them 12 states with $J^\pi=1^-$, 19 with 2^-, and 25 with 3^- that can be populated in the Ho 2^- decay. Here, an interesting result is that the lowest-lying states of these spin values are the three lowest levels of the entire configuration. This result is a consequence of the dominant component in these levels of the $(\pi h_{11/2}\nu h_{9/2})_{1^+}$ two-body coupling with the large residual attraction of -1.349 MeV (Table III). Theoretically, the same component is exclusively fed in $(\pi h_{11/2}^2)_{0^+}\rightarrow(\pi h_{11/2}\nu h_{9/2})_{1^+}$ GT-decay of ^{150}Ho, and thus the dominant fraction of this β decay will proceed to these three lowest-lying levels, which are predicted in the calculation at 4.316, 4.453, and 4.474 MeV for spin 1^-, 3^-, and 2^- and should receive $>99\%$, $>99\%$, and 92% of the decay strength, respectively.

This latter theoretical result is in conflict with that of the experiment, where for each spin several states are strongly fed, and around 170 levels are identified in the 3.8–5.9-MeV interval including the resonance. But the anticipated high level-density near 4.4 MeV excitation in ^{150}Dy for $J^\pi=1^-$, 2^-, and 3^- will give rise to complex, nonspecific mixing with the respective GT states. The configuration mixing, however, will preserve the original centroid energy of the strength. We therefore list in Table IV the strength-weighted, average energies for each spin. We should note here that the centroids are mainly determined by four to six strongly fed levels for each spin. Their agreement with our parameter-free, theoretical prediction is excellent (within 75 keV), and it strongly supports the GT character of the observed resonance.

For detailed calculations of the decay strength we need the composition of the ^{150}Ho 2^- parent state. We obtained it from a similar four-nucleon calculation using the pertinent input data from Table III, now requiring the three protons in the $s_{1/2}$, $d_{3/2}$, or $h_{11/2}$ and the neutron in the $f_{7/2}$ orbital. In this case two protons can couple to 0^+, and we therefore need the respective diagonal and off-diagonal 0^+ pairing matrix elements explained before.

One result of this calculation is the distribution for the two-proton 0^+ pair, which results as 76% $h_{11/2}^2$, 17% $s_{1/2}^2$, and 7% $d_{3/2}^2$, in satisfactory agreement with the elementary expectation from pair degeneracy of $\frac{6}{8}:\frac{1}{8}:\frac{1}{8}$. The 76% pair occupation of the $h_{11/2}$ orbital enters directly in the calculation of the total GT strength of the ^{150}Ho 2^- decay. The fundamental theoretical relation gives $B_{GT}(^{150}\mathrm{Ho}_{2^-})=n\ 4l/2(l+1)g_A^2/4\pi=2.76g_A^2/4\pi$ as listed in Table IV, where now the number of particles n is equal to 1.52. The large discrepancy with the experimental result of $0.241g_A^2/4\pi$, also given in Table IV, is well known from other studies, and is often referred to as the Gamow-Teller quenching. For example, a quite closely related neighboring case is the ^{148}Dy GT decay [7], representing the similar decay of two paired $h_{11/2}$ protons. Here, the theoretical strength is $2.4g_A^2/4\pi$, again taking into account the $h_{11/2}$ pair occupancy, $\sim 2/3$ in this case, compared to the experimental result of $0.44(3)\ g_A^2/4\pi$. However, we know that the present experiment is not the ideal one for evaluating the full B_{GT} strength inside the window (see Sec. V).

A second theoretical prediction is the spin distribution of the GT strength. The shell-model (SM) analysis explicitly calculates these quantities and gives $^{SM}B_{GT}^{1^-}:{}^{SM}B_{GT}^{2^-}:{}^{SM}B_{GT}^{3^-}=3.6:4.0:7.4$ (normalized to 15 arbitrary units), in excellent agreement with our measured result of $^{Expt.}B_{GT}^{1^-}:{}^{Expt.}B_{GT}^{2^-}:{}^{Expt.}B_{GT}^{3^-}=3.4:4.2:7.4$, also given in Table III, but there in units of $g_A^2/4\pi$. This result confirms our J^π assignments to the levels as well as our interpretation of the resonance.

V. SUMMARY AND CONCLUSIONS

As stated in the Introduction a comparison of a high-sensitivity γ ray study of β-decay using state-of-art-detectors, such as that presented here, with results obtained using the TAS technique can provide essential information on the advantages and limitations of both methods. The results of the TAS measurements will be given in a forthcoming publication [6]. Here we will only compare some general results obtained with both techniques. The high-resolution technique fails to reveal β feeding to levels at excitation energy higher than 5.9 MeV. This failure has drastic consequences in the determination of the full β strength. Missing feeding to levels at high excitation energy has the consequence that apparent feeding is attributed to levels at low excitation energy, and the β-feeding distribution is correspondingly distorted over the whole energy range. The difference is clearer in terms of numbers: the total B_{GT} obtained from the present CLUSTER CUBE measurement is 0.267 ($\log_{10} ft=4.16$) and the B_{GT} obtained from the TAS experiment in the same range of energy (0–5.9 MeV) is 0.455 ($\log_{10} ft=3.93$), which represents 70% more B_{GT}. In total the TAS results give 116% more B_{GT} [5].

The reasons for the experimental limitations of the high-resolution technique are well understood: (a) low photopeak

efficiency of Ge detectors (valid even for state-of-the-art detectors) for γ rays of high energy, (b) fragmentation of the β strength (or β feeding) at high excitation energy caused by the increasing level density, and (c) fragmentation of the deexcitation of the levels through many different cascades. Due to these effects many weak cascades that deexcite a level at high excitation energy can remain undetected, leading to systematic errors in the determination of the strength. The magnitude of the problem, known as the Pandemonium effect [17], can be reduced with the use of more efficient detectors, as we have done here, but presently cannot be completely avoided if high-resolution techniques are used. For example, prior to our work, only five levels and 4 γ rays were known from the decay of the ^{150}Ho 2^- isomer [18]. These numbers should be compared with the 295 levels and 1064 γ rays observed in this work. Thus, better detectors give better results, but the problem still remains, and what is even worse, the magnitude of the problem depends on each particular case.

The solution to this problem is the use of the total absorption technique which, with proper techniques of analysis [5,6], can give reliable results for the β strength. The main disadvantage of the TAS technique is the lack of detailed spectroscopic information that can be gained using high-resolution techniques (spins, parities, number of levels). Consider, for example, that a very important result of the present experiment is the fact that underneath a clear resonance revealed in total absorption experiments we observed a large number of levels still well separated experimentally. Unique to the present case is the fact that the spin-parity assignments to many of the levels can be made based only on the GT selection rules and the electromagnetic properties of the decay of the levels. It is also remarkable that we can interpret the global properties of these levels in terms of a simple and parameter free shell-model calculation. The excitation energies of the strength-weighted centroids of all levels in the 3.5–5.9 MeV energy interval with spins 1^-, 2^-, and 3^- are well predicted by the shell-model calculation. Equally well reproduced is the relative distribution of the strength allocated to each particular spin. A clear difference between experiment and theory is observed regarding the number of levels detected, four times more than that calculated as well as the distribution of the strength among states of the same spin parity. In the experiment most of the strength is concentrated in a few levels of each spin, while in theory most of the strength is concentrated in one level of each spin. This is, however, to be expected since the shell-model calculation is restricted to a particular configuration (the one relevant to GT decay), while many other configurations giving the same J^π might exist at this high excitation energy. The spreading of the strength is then due to small and probably unspecified admixtures among all these levels.

ACKNOWLEDGMENTS

The authors thank Professor Peter Kleinheinz for many useful discussions. This work was partially supported by the CICYT (Spain) under Contract No. FPA 2002-04181-C04-03, by the CSR (Poland) Grant No. KBN-2Pp03B-039-13, by the RFBR-DFG (Germany) Contract No. 436 RUS 113/201/0(R), by the EC Contract No. HPMF-CT-1999-00394, and by MEC Contract No. SAB1995-0619.

APPENDIX

The two-body interactions used in the calculations [relations (A1)–(A8)] are estimated as the difference between the experimental excitation energies of a given configuration with an appropriate J^π (E^* in the pertinent nucleus) and the unperturbed energies, neglecting the residual interactions (inside square brackets). We note here that the unperturbed energies are calculated using single-particle energies and ground state masses following the philosophy explained in Ref. [19]. The masses are given schematically in boxes (mass windows) where the double frame corresponds to the mass of the ^{146}Gd core. The masses are taken from Ref. [20], except for the 148-mass chain which has been slightly modified (reduced) by 30 keV [16].

Thus two-proton matrix elements[1]

$$\begin{aligned} <\pi h_{11/2}^2|V|\pi h_{11/2}^2>_{2^+,..\,10^+} &= E^*_{2^+,..\,10^+}(^{148}Dy) - [2E^*(\pi h_{11/2}\ ^{147}Tb) + \begin{array}{|c|}\hline -1 \\ \hline +2 \\ \hline -1 \\ \hline \end{array}\,] \\ &= E^*_{2^+,..\,10^+}(^{148}Dy) - 2542\ keV \end{aligned} \tag{A1}$$

$$\begin{aligned} <\pi h_{11/2}\pi s_{1/2}|V|\pi h_{11/2}\pi s_{1/2}>_{5^-,..\,6^-} &= E^*_{5^-,..\,6^-}(^{148}Dy) - [E^*(\pi h_{11/2}\ ^{147}Tb) + E^*(\pi s_{1/2}\ ^{147}Tb) \\ &\quad + \begin{array}{|c|}\hline -1 \\ \hline +2 \\ \hline -1 \\ \hline \end{array}\,] \\ &= E^*_{5^-,..\,6^-}(^{148}Dy) - 2491\ keV \end{aligned} \tag{A2}$$

[1] $\langle \pi^2|V|\pi^2\rangle_{0^+}$ matrix elements are explained in the text.

$$< \pi h_{11/2}\pi d_{3/2}|V|\pi h_{11/2}\pi d_{3/2} >_{4^-,..\,7^-} = E^*_{4^-,..\,7^-}(^{148}Dy) - [E^*(\pi h_{11/2}\,{}^{147}Tb) + E^*(\pi d_{3/2}\,{}^{147}Tb) + \boxed{\begin{array}{|c|}\hline -1 \\ \hline +2 \\ \hline -1 \\ \hline \end{array}}\,] = E^*_{4^-,..\,7^-}(^{148}Dy) - 2744\ keV \tag{A3}$$

Proton-neutron matrix elements

$$< \pi h_{11/2}\nu f_{7/2}|V|\pi h_{11/2}\nu f_{7/2} >_{2^+,..\,9^+} = E^*_{2^+,..\,9^+}(^{148}Tb) - [E^*(\pi h_{11/2}\,{}^{147}Tb) + E^*(\nu f_{7/2}\,{}^{147}Gd) + \boxed{\begin{array}{|c|c|}\hline +1 & -1 \\ \hline -1 & +1 \\ \hline \end{array}}\,] = E^*_{2^+,..\,9^+}(^{148}Tb) - 572\ keV \tag{A4}$$

$$< \pi s_{1/2}\nu f_{7/2}|V|\pi s_{1/2}\nu f_{7/2} >_{3^-,..\,4^-} = E^*_{3^-,..\,4^-}(^{148}Tb) - [E^*(\pi s_{1/2}\,{}^{147}Tb) + E^*(\nu f_{7/2}\,{}^{147}Gd) + \boxed{\begin{array}{|c|c|}\hline +1 & -1 \\ \hline -1 & +1 \\ \hline \end{array}}\,] = E^*_{3^-,..\,4^-}(^{148}Tb) - 521\ keV \tag{A5}$$

$$< \pi d_{3/2}\nu f_{7/2}|V|\pi d_{3/2}\nu f_{7/2} >_{2^-,..\,5^-} = E^*_{2^-,..\,5^-}(^{148}Tb) - [E^*(\pi d_{3/2}\,{}^{147}Tb) + E^*(\nu f_{7/2}\,{}^{147}Gd) + \boxed{\begin{array}{|c|c|}\hline +1 & -1 \\ \hline -1 & +1 \\ \hline \end{array}}\,] = E^*_{2^-,..\,5^-}(^{148}Tb) - 774\ keV \tag{A6}$$

Two neutron matrix elements

$$< \nu f^2_{7/2}|V|\nu f^2_{7/2} >_{0^+,..\,6^+} = E^*_{0^+,..\,6^+}(^{148}Gd) - [2E^*(\nu f_{7/2}\,{}^{147}Gd) + \boxed{\begin{array}{|c|c|c|}\hline -1 & +2 & -1 \\ \hline \end{array}}\,] = E^*_{0^+,..\,6^+}(^{148}Gd) - 1642\ keV \tag{A7}$$

$$< \nu f_{7/2}\nu h_{9/2}|V|\nu f_{7/2}\nu h_{9/2} >_{1^+,..\,8^+} = E^*_{1^+,..\,8^+}(^{148}Gd) - [E^*(\nu f_{7/2}\,{}^{147}Gd) + E^*(\nu h_{9/2}\,{}^{147}Gd) + \boxed{\begin{array}{|c|c|c|}\hline -1 & +2 & -1 \\ \hline \end{array}}\,] = E^*_{1^+,..\,8^+}(^{148}Gd) - 3039\ keV \tag{A8}$$

Mass window for calculating excited states in ^{150}Dy using the matrix elements given above:

$$S = \boxed{\begin{array}{|c|c|c|}\hline & & -1 \\ \hline +2 & & \\ \hline -3 & +2 & \\ \hline \end{array}} = 5362\ \ keV \tag{A9}$$

[1] A. Algora, D. Cano-Ott, B. Rubio, J.L. Tain, J. Agramunt, J. Blomqvist, L. Batist, R. Borcea, R. Collatz, A. Gadea, J. Gerl, M. Gierlik, M. Górska, O. Guilbaud, H. Grawe, M. Hellström, Z. Hu, Z. Janas, M. Karny, R. Kirchner, P. Kleinheinz, W. Liu, T. Martinez, F. Moroz, A. Płochocki, M. Rejmund, E. Roeckl, K. Rykaczewski, M. Shibata, J. Szerypo, V. Wittman, and German Euroball Collaboration, Nucl. Phys. **A654**, 727c (1999).

[2] J. Agramunt, A. Algora, D. Cano-Ott, A. Gadea, B. Rubio, J.L.

Tain, M. Gierlik, M. Karny, Z. Janas, A. Płochocki, K. Rykaczewski, J. Szerypo, R. Collatz, J. Gerl, M. Górska, H. Grawe, M. Hellström, Z. Hu, R. Kirchner, M. Rejmund, E. Roeckl, M. Shibata, L. Batist, F. Moroz, V. Wittman, and P. Kleinheinz, in *Proceedings of the International Symposium on New Facet of Spin Giant Resonances in Nuclei, Tokyo, 1997*, edited by H. Sakai, H. Okamura, and T. Wakasa (World Scientific, Singapore, 1998), p. 150.

[3] Z. Hu, L. Batist, J. Agramunt, A. Algora, B.A. Brown, D. Cano-Ott, R. Collatz, A. Gadea, M. Gierlik, M. Górska, H. Grawe, M. Hellström, Z. Janas, M. Karny, R. Kirchner, F. Moroz, A. Płochocki, M. Rejmund, E. Roeckl, B. Rubio, M. Shibata, J. Szerypo, J.L. Tain, and V. Wittman, in *ENAM 98, Exotic Nuclei and Atomic Masses*, edited by Bradley M. Sherrill, David J. Morrisey, and Cary N. Davids, AIP Conf. Proc. No. 455 (AIP, Woodbury, NY, 1998), p. 769; Z. Janas, J. Agramunt, A. Algora, L. Batist, B.A. Brown, D. Cano-Ott, R. Collatz, A. Gadea, M. Gierlik, M. Górska, H. Grawe, A. Gulielmenti, M. Hellström, Z. Hu, M. Karny, R. Kirchner, F. Moroz, A. Piechaczek, A. Płochocki, M. Rejmund, E. Roeckl, B. Rubio, K. Rykaczewski, M. Shibata, J. Szerypo, J.L. Tain, V. Wittman, and A. Wöhr, *ibid.*, p. 725.

[4] Z. Hu, L. Batist, J. Agramunt, A. Algora, B.A. Brown, D. Cano-Ott, R. Collatz, A. Gadea, M. Gierlik, M. Górska, H. Grawe, M. Hellström, Z. Janas, M. Karny, R. Kirchner, F. Moroz, A. Płochocki, M. Rejmund, E. Roeckl, B. Rubio, M. Shibata, J. Szerypo, J.L. Tain, and V. Wittman, Phys. Rev. C **60**, 024315 (1999); **62**, 064315 (2000).

[5] D. Cano-Ott, Ph.D. thesis, University of Valencia, 2000; D. Cano-Ott and J. L. Tain (unpublished).

[6] D. Cano-Ott *et al.* (unpublished).

[7] P. Kleinheinz, K. Zuber, C. Conci, C. Protop, J. Zuber, C.F. Liang, P. Paris, and J. Blomqvist, Phys. Rev. Lett. **55**, 2664 (1985).

[8] J. Eberth, H.G. Thomas, P.v. Brentano, R.M. Lieder, H.M. Jäger, H. Kämmerling, M. Berst, D. Gutknecht, and R. Henck, Nucl. Instrum. Methods Phys. Res. A **369**, 135 (1996).

[9] J. Gulyás, computer code ELEVEN (MTA Atowki, Debrecen, unpublished).

[10] E. der Mateosian and J.K. Tuli, Nucl. Data Sheets **75**, 960 (1995).

[11] D. Beck, F. Ames, G. Audi, G. Bollen, H.-J. Kluge, A. Kohl, M. Knig, D. Lunney, I. Martel, R.B. Moore, H. Raimbault-Hartmann, E. Schark, S. Schwarz, M. de Saint Simon, and J. Szerypo, Nucl. Phys. **A626**, 343c (1997).

[12] M. Lach, P. Kleinheinz, M. Piiparinen, M. Ogawa, S. Lunardi, M.C. Bosca, J. Styczen, and J. Blomqvist, Z. Phys. A **341**, 25 (1991).

[13] C. Zhang, Ph.D. thesis, Univ. Köeln, Germany, Report Julich-2857, 1993.

[14] J. Styczen, P. Kleinheinz, W. Starzecki, B. Rubio, G. de Angelis, H.J. Hähn, C.F. Liang, P. Paris, R. Reinhardt, P. von Brentano, and J. Blomqvist, in *Nuclei Far from Stability*, edited by I. S. Towner, AIP Conf. Proc. No. 164 (AIP, New York, 1988), p. 489.

[15] J.L. Taín, B. Rubio, P. Kleinheinz, D. Schardt, R. Barden, and J. Blomqvist, Z. Phys. A **333**, 29 (1989).

[16] J. Blomqvist (private communication).

[17] J.C. Hardy, L.C. Carraz, B. Jonson, and P.G. Hansen, Phys. Lett. **71B**, 307 (1977).

[18] C.F. Liang, P. Paris, A. Peghaire, and H. Szichman, Z. Phys. A **297**, 303 (1980); D.M. Moltz, K.S. Toth, Y.A. Ellis-Akovali, and J.D. Cole, Phys. Rev. C **26**, 1316 (1982); E. Nolte, S.Z. Gui, G. Colombo, G. Korschinek, and K. Eskola, Z. Phys. A **306**, 223 (1982); K.S. Toth, D.C. Sousa, J.M. Nitschke, and P.A. Wilmarth, Phys. Rev. C **35**, 620 (1987).

[19] J. Blomqvist, P. Kleinheinz, and P.J. Daly, Z. Phys. A **312**, 27 (1983).

[20] G. Audi and A.H. Wapstra, Nucl. Phys. **A624**, 1 (1997).